Biointerface Research in Applied Chemistry
Platinum Open Access Journal (ISSN: 2069-5837)

Article
Volume 11, Issue 4, 2021, 11856 - 11890
https://doi.org/10.33263/BRIAC114.1185611890

Biological Potency of New Benzimidazole Derived Imine Based Ligand and its Co(III), Ni(II), Cu(II) and Pt(II) Complexes: Synthesis, Structure, Antimicrobial, Antioxidant and BSA Interaction Studies

Prakasha Gavisiddegowda [1], Divyashree Nallur Rajashekhar [1], Shiva Prasad Kollur [2], Revanasiddappa Hosakere Doddarevanna [1,*]

[1] Department of Chemistry, University of Mysore, Manasagangotri, Mysuru – 570 006, Karnataka, India
[2] Department of Sciences, Amrita School of Arts and Sciences, Amrita Vishwa Vidyapeetham, Mysuru Campus, Mysuru – 570 026, Karnataka, India
* Correspondence: hdrevanasiddappa@yahoo.com;

Scopus Author ID 7004879365
Received: 18.11.2020; Revised: 15.12.2020; Accepted: 16.12.2020; Published: 18.12.2020

Abstract: In this study, we report the synthesis and characterization of transition metal complexes (MC1, MC2, MC3, MC4) where M= Co(III), Ni(II), Cu(II) and Pt(II), respectively, using a new imine-based ligand, 2-{(E)-[(1H-benzimidazol-2-ylmethyl)imino]methyl}-4-bromophenol (HBMB). The molecular structure of the HBMB ligand and its complexes were confirmed by various analytical techniques such as UV-Vis, FT-IR, ^{1}H, ^{13}C-NMR, ESR, TGA/DTA, LC-MS, molar conductance, and magnetic moment measurements. The spectral data of complexes recommended tridentate binding modes of HBMB ligand and suggested an octahedral geometry for MC1 and MC2 complexes while square planar geometry for MC3 and MC4 complexes. Further, the biological activities viz., antimicrobial, antioxidant, and BSA interaction studies were performed using the prepared compounds. The antimicrobial activity results suggested that all the synthesized transition metal complexes showed significant antimicrobial activity against several bacterial and fungal species compared with standard drug and the parent ligand, HBMB. The interaction of metal complexes with BSA (Bovine serum albumin) was performed. The results strongly recommended among the synthesized complexes, platinum complex (MC4) showed marked interaction with the BSA protein. It also indicates that the probable quenching mechanism of BSA fluorescence by complexes is a static quenching procedure, and the spontaneous binding interaction is mainly entropy driven with either van der Waals force or hydrogen binding reaction. The free radical scavenging ability of test samples was assessed using *an in vitro* assay viz., DPPH.

Keywords: Benzimidazole; transition metal complexes; BSA interaction; antimicrobial activity;

1. Introduction

The compounds bearing azomethine group (imine base) has attracted a huge number of chemists and biochemists [1-3] due to their ease of synthesis, high affinity to form complexes with metal ions (metal atom), high stability, their pharmacological activity, and marked anticancer properties [4]. The various geometries were possessed by the transition metal complexes changing their coordination number that is not feasible for purely organic moieties. Their oxidation states are the tunable properties, which is another excellent advantage [5]. Some transition metal ions such as copper(II), nickel(II), and platinum(II) have notable

biological activity [6]. Therefore, Cu(II) complexes mimic cis-platin and the significance of copper in the catalytic activity of some enzymatic reactions [6]. Cobalt indirectly displayed a great role in DNA synthesis. It is a vital biological element in the cobalt-reliant proteins [6]. The complexes containing Co(III) ion was most favored in coordination chemistry and biomedical area due to their therapeutic properties [7]. The nickel-metal ion plays an important role in urease's characterization as a nickel enzyme since 1975 in bioinorganic chemistry has been immediately reviewed [8]. The binding interaction of nickel complexes with the DNA constructs mainly depends on the ligand's structural features associated with intercalative nature [9]. Recently, some square planar Pt(II) complexes with comparatively high antitumor activity and low renal toxicity (e.g., iproplatin and JM216) have been popularized [10], promoting cancer cell death with a mechanism different from the other metal complexes and remain to induce against cisplatin-resistant cancer cell line [11]. In the present investigation, platinum complex bearing benzimidazole tridentate nitrogen and oxygen donor/ halogenated ligands serving as the leaving groups have been designed. The binding constants, binding sites, and thermodynamic force exist between the resultant transition metal complexes, and BSA was discussed based on recorded spectroscopic data. The obtained results were strongly recommended in drug delivery. Drug design BSA procedures are a notable water-soluble protein and maintained in several biological functions. It generally controls or maintains the osmotic pressure, blood pH level and stabilize the concentration of the metal ion in the body [12, 13]. The blood circulatory system also helps excrete and promote many small molecules to definite targets [14, 15]. *In-vitro* approach, BSA was selected to study the interaction of drug-protein.

2. Materials and Methods

All the reagents and chemicals are procured from commercial sources (Merck, India) and used without purification. The synthesized compounds' melting points were recorded by using a precision digital point apparatus and are uncorrected. Perkin Elmer 240 CHN-analyzer was used for measuring the elemental composition of the prepared compounds. UV-Visible spectra were measured on ELICO SL-117 double beam spectrophotometer in the region between 200 and 800 nm. Infrared spectral studies were performed using Perkin Elmer spectrum version 10.03.09 between 4000 and 400 cm^{-1}. ^{1}H and ^{13}C NMR spectra of the heterocyclic ligand were recorded on a Bruker 400 MHz spectrometer. TMS is used as standard reference material. Thermal investigation of the transition metal complexes was studied on a Diamond TG/DT analyzer from ambient temperature to 800 °C with the heating rate at 10 °C/min at a sophisticated analytical instruments facility at the University of Mysore. The ligand and its complexes' molecular mass was confirmed on LC-MS/MS Synapt G2 HDMS through LC-MS spectroscopy at Centralized Instrumentation Facility, University of Mysore. The copper complex's paramagnetic behavior (ESR) was scanned on a JEOL X-Band at 77 K under liquid nitrogen and TCNE (Tetracyanoethylene) as the g-marker. Molar conductance of the complexes was measured on Elico CM-180 conductometer with a cell having cell constant 1. The magnetic property of the transition metal complexes resolved on Guoy's balance and $Hg[Co(SCN)_4]$ used as a standard material.

2.1. Chemical synthesis.

2.1.1. Synthesis of 2-{(E)-[(1H-benzimidazol-2-ylmethyl)imino]methyl}-4-bromophenol (HBMB).

The heterocyclic imine based ligand, HBMB was synthesized using a method described earlier [16]. The equimolar mixture of aqueous 2-(aminomethyl) benzimidazole hydrochloride solution (0.100 g, 0.5573 mmol) and an aqueous solution of potassium carbonate (0.0803 g, 0.6431 mmol) were neutralized in the first step, followed by the addition of 5- bromo-salicyladihyde (0.0737 g, 0.5533 mmol). The resulting mixture was continuously stirred at room temperature for 1 h using a magnetic stirrer. The obtained yellow precipitate was washed with water, followed by petroleum ether, and dried under vacuum. The reaction completion was monitored on pre-coated silica gel plates by the TLC method using chloroform and methanol as a solvent system in the ratio (9:1). The final product thus obtained was insoluble in water but soluble in methanol and DMSO.

Elemental analysis for HBMB ($C_{15}H_{11}BrN_3$) Found (%) C, 54.56; H, 3.66; Br, 24.20; N, 12.73; O, 4.85**.** ^{1}H NMR (DMSO-d_6, 400 MHz) ð: 5.00 (s, 2H, CH2), 6.84-6.93 (d, 1H, Ar-H), 7.13-7.14 (t, 2H, Ar-H), 7.40-7.43(d, 1H, Ar-H), 7.45-7.53(d, 1H, Ar-H), 7.74-7.75, (d, 1H, Ar-H), 7.86-7.87 (s, 1H, Ar-H), 8.72 (s, 1H,N=CH), 12.49(s,1H, NH in imidazole ring), 12.95 (1H, Ar-OH). ^{13}C NMR (DMSO-d_6, 100 MHz) ð: 115.27, 115.95, 116.79, 117.02, 118.08, 118.15, 118.92, 120.17, 120.41, 122.96, 123.15, 150.27, 154.31, 156.78, 167.67 ppm. ESI-LCMS *m/z*: calcd. for $C_{15}H_{11}BrN_3O$), 330.18; found 331.89 (M+1) (s18.S1, S6, S11 and S16-S17)

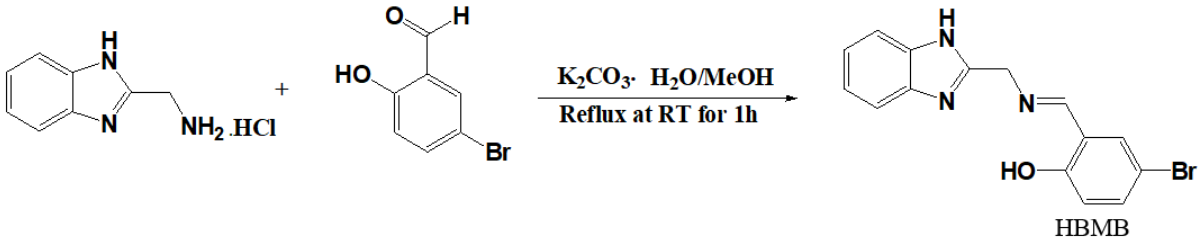

Scheme 1. Synthesis of 2-{(E)-[(1H-benzimidazol-2-ylmethyl)imino]methyl}-4-bromophenol (HBMB).

2.1.2. Synthesis of 2-{(E)-[(1H-benzimidazol-2-ylmethyl)imino]methyl}-4-bromophenol complexes containing Co(III) and Ni(II) [MC1 and MC2].

The heterocyclic imine based complexes containing Co(III) and Ni(II) were synthesized by adding the hot methanolic solution of metal chloride ($CoCl_2$.$6H_2O$ and $NiCl_2$ ·$6H_2O$) to a methanolic solution of heterocyclic imine base ligand (HBMB). The resulting mixtures were reflux for 6 to 7 hours on a water bath to get a brown and red color precipitate of cobalt and nickel complexes, respectively.

2.1.3. Synthesis of 2-{(E)-[(1H-benzimidazol-2-ylmethyl)imino]methyl}-4-bromophenol complexes Containing Cu(II) and Pt(II) [MC3 and MC4].

Cu(II) and Pt(II) complexes were synthesized by adding the hot methanolic solution of metal chloride ($CuCl_2$.$2H_2O$ and $PtCl_2$·$2H_2O$) to a methanolic solution of heterocyclic imine base ligand (HBMB). The resulting mixtures were reflux for 6 to 7 hours on a water bath to get a green and orange color precipitate of copper and platinum complexes, respectively.

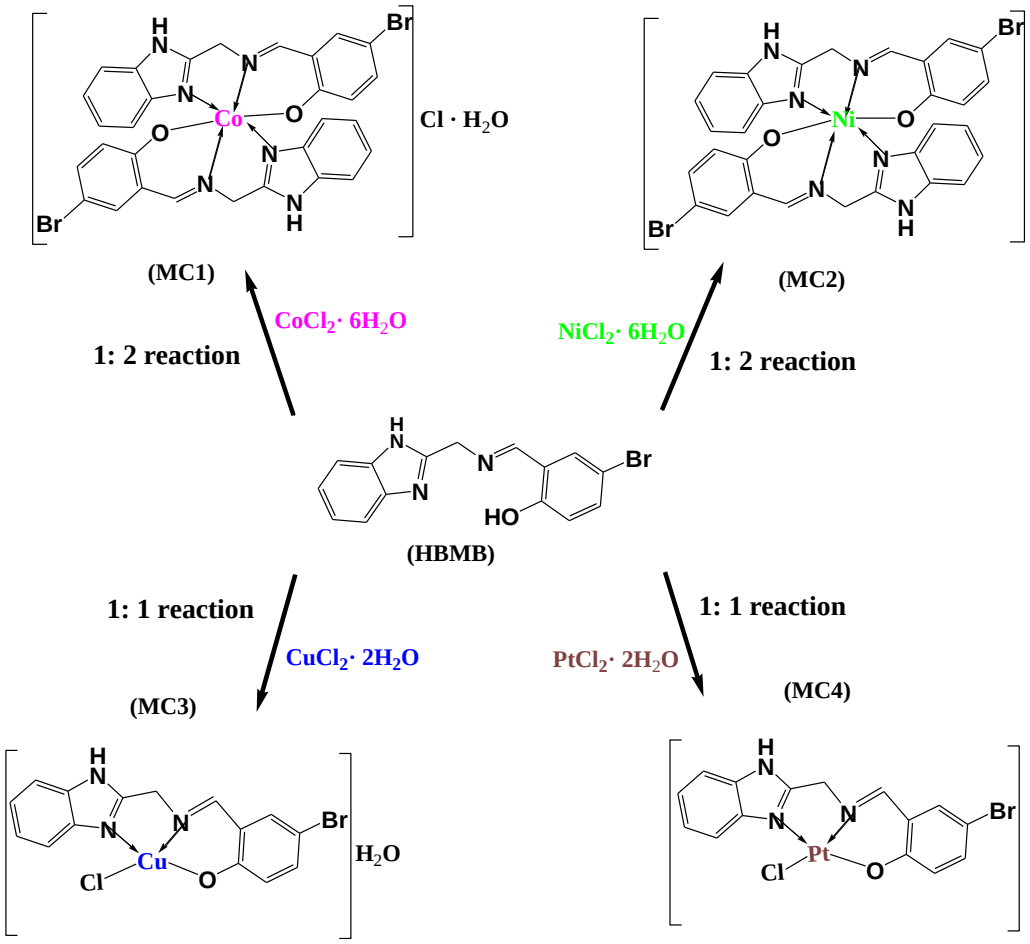

Figure 1. Proposed structures and synthetic rout of metal the complexes MC1-MC4.

2.2. Biological studies.

2.2.1. Antimicrobial activity.

The newly prepared ligand (HBMB) and its transition metal complexes (MC1-MC4) were tested against some Gram-negative and Gram-positive bacteria to estimate their antibacterial efficacy. Gram-positive strains, *Listeria monocytogenes* (ATCC 13593), *Staphylococcus aureus* (ATCC 700699) and *Bacillus subtilis* (ATCC 21332), and Gram-negative strains, *Escherichia coli* (ATCC 0157:H7), *Vibrio cholera* (ATCC 212001), and *Pseudomonas aeruginosa* (ATCC 15442) were used in this studies. The suspension of inoculum was standardized to 10^6 colony-forming units of bacteria. Each synthesized transition metal complex and ligand stock solution (1000 mg/mL) were prepared separately in dimethyl sulfoxide (DMSO, v/v). The good diffusion method was used to study the qualitative bacterial activity [17]. The prepared inoculums of bacterial were spread evenly with a sterile L-shaped glass rod onto an agar plate of Muller-Hinton. The sterile cork borer was used to prepare the wells (9 mm in diameter) 100 µL of the test compounds were added to each well. Then incubation of each plate and were kept for 24 h at 37 °C. After incubation, around each well was measured the zone of inhibition (in mm).

The disc diffusion method was used to perform the *in vitro* antifungal activity of synthesized complexes (MC1-MC4) and the parent ligand (HBMB) [18]. *Aspergillus flavus and Aspergillus niger* have been employed for the present study, cultured on a medium of potato dextrose agar (PDA). Approximately 9mm in diameter well was made at the center of agar medium in the typical procedure, which was previously inoculated in the presence of

fungi. The tested solutions (100 µL) were filled with well using a micropipette, and the plate was incubated at 37 °C for 72 h. In the meanwhile, diffuse the test solution and the inoculated fungi was growth with affected. Measure the development of the inhibition zone on the plate. Fluconazole was used as a reference compound for the studies.

2.2.2. Minimum inhibitory concentration (MIC).

The obtained novel benzimidazole ligand and its transition metal complexes were screens for their MIC assay in DMSO by serial plate dilution method [19]. The nutrient broth, containing the logarithmic serially two-fold diluted magnitude of the test compounds and controls, was inoculated with approximately 10^4 c.f.u mL^{-1}(colony composing unit) of actively dividing bacterial cells. The cultures were incubated for 24 h at 37 ^{0}C, and magnification was monitored visually and spectrophotometrically at 600 nm. The lowest concentration (highest dilution) required to apprehend bacteria's magnification was regarded as minimum inhibitory concentration (MIC).

2.2.3. Antioxidant activity: free radical scavenging activity by DPPH assay.

DPPH containing an odd electron with a very strong absorption peak at 517 nm. When the unpaired electron in the DPPH moiety becomes paired off, the absorption stoichiometrically decreases, concerning the number of electrons utilized. Such a variation in the absorbance produced in the resultant reaction has been widely using to analyze several molecules' capacity as free radical scavengers. The radical-scavenging or hydrogen donating ability providing the stable radical DPPH was used to record the ligand's free radical-scavenging activity and its complexes illustrated by the Blois method [20]. The sample stock solutions (0.001g/mL) were prepared by dissolving a suitable amount of DPPH in DMSO. Change in concentrations (0.2-1.0×10^{-2} µL) of stock solution was made up to 3 mL with methanol. DPPH solution was utilized for the above-tested solutions. The obtained mixture was shaken well and incubated for 30 min, and measured the absorbance at 517 nm. All the estimates were run in triplicate, and mean ± standard deviation (S. D) was used to express the results. Ascorbic acid was the standard or positive for the experiment, parallel to the test compound and without test compound or standard used as the negative control. The following equation was used to calculate the capability to scavenge the DPPH radical:

$$I\ (\%) = (A_{blank} - A_{sample}/A_{blank}) \times 100$$

where A_{blank} is the absorbance of the control reaction mixture with the test compounds, $A_{samples}$ is the absorbance of the test compounds.

2.2.4. BSA interaction.

The aqueous solution containing 10 mM Tris-HCl buffer (pH 7.3) was used to dissolve the bovine serum albumin at room temperature. The prepared solution was kept in the dark condition and used soon after. The protein concentration was spectrophotometrically using an extinction coefficient at ε 280 of 44300 $M^{-1}cm^{-1}$ [21]. The complexes MC1 to MC4 stock solutions were prepared in DMSO, and tris buffer was used to dilute the solution up to mark.

2.2.4.1. Electronic studies.

The BSA concentration was kept constant at 10µM. While the concentration of the resultant complexes varied from 5-25 µM presence of aqueous tris buffer.

2.2.4.2. Fluorescence measurements.

The compounds binding to BSA were qualitatively analyzed by a fluorescence quenching method. The decrease in the quantum yield of a fluorophore fluorescence influenced by an interaction of various molecules with a quencher molecule is analyzed. Fluorescence studies were measured on a Model F-2000 Hitachi spectrofluorometer equipped with a 150 W Xenon lamp at a different temperature at 298, 303, and 310 K. Both excitation and emission light were set the bandwidth about of 5.0 nm. A very dilute BSA solution (20×10^{-5} mol/L) and MC1-MC4 ($0.0\text{-}60.0\times10^{-5}$ mol/L) were used to perform. The excitation was carried out at 350 nm, and the emission was scanned from 370 to 570 nm. A quencher absorption at the wavelength of emission and excitation of a fluorophore significantly affects the fluorescence spectra. Therefore, all intensities of fluorescence were corrected to absorb exciting light and light of emitted re-absorption based on the below equation (1).

$$F_{corr} = F_{obs}\, e^{(A_{ex}+Aem)^2} \quad (1)$$

where, F_{corr} and F_{obs} are the corrected and absorbed fluorescence intensities, respectively. A_{ex} and A_{obs} are the absorption of the system at the excitation and emission wavelengths, respectively.

3. Results and Discussion

3.1. Chemistry.

3.1.1. Physico-chemical characterization.

Based on the physicochemical studies, synthesized imine-based moiety act as a tridentate ligand containing nitrogen and oxygen donor atoms while synthesized cobalt and nickel complexes are in 1:2 (M:L) ratio similarly, copper and platinum complexes are in 1:1 (M:L) ratio. Dissolve the resultant transition metal complexes in DMSO and made them with a millimolar solution. The above millimolar solution was used to measure the conductance of synthesized metal complexes at room temperature and compare it with the free metal ion solution. The steady decrease in the value of molecular conductance attributed to complexes' formation, and all the complexes are stable in solution state was confirmed by a constant conductance at different time intervals. The presence of halogen ion outside the coordination sphere is confirmed by huge conductance in the MC1 complex. While the other transition metal complexes are non-electrolytes with low or zero conductance, as shown in Table 1.

Table 1. Elemental analysis of synthesized compounds.

Compound	C	H	N	O	Cl	Br	Metal ion
HBMB	54.56	3.66	12.73	4.85	-	20.24	-
MC1	46.75	3.14	10.90	6.23	4.60	20.73	7.65
MC2	50.25	3.09	10.90	4.48	-	2073	7.64
MC3	40.38	2.94	9.42	7.17	7.95	17.91	14.24
MC4	32.19	1.98	7.51	2.86	6.33	14.28	34.88

Further, as shown in Table 2, the paramagnetic behavior of Cu(II)-imine based metal complex exhibited a magnetic moment between 1.89 and 1.95 B.M., which is higher than that of the 1.73 BM (spin-only value). The high-field and low-field complexes of a few 3d-series metal ions vary in the number of unpaired electrons in the complexes when this quantity can be analyzed more easily from a comparison of the calculated magnetic moment from the low-field and high-field complexes and that of the measured magnetic moment. The number of

unpaired electron calculations gives the details about the oxidation state of a complex containing a metal ion. Meanwhile, investigating the geometry of several complexes, the magnetic moment value (1.93 BM) supported the square planar geometry around the resultant Cu(II) complex. The magnetic moment value was not observed for the resultant cobalt(III) complex, which strongly recommends the strong field $3d^6 4s^0$ diamagnetic nature of the synthesized cobalt complex. The magnetic moment value and spectral value were supported by the octahedral environment around the Co(III) complex. The octahedral Ni(II) complexes always show the magnetic moment value range from 2.91 to 3.96 B.M. [22]. In the resultant Ni(II) Schiff base complex, the magnetic moment was obtained to be 3.18 B.M. This reveals that the complex is suitable for octahedral geometry. On the other hand, the square planar environment was around the Pt(II) ion. The zero magnetic moment value was registered for the prepared platinum complex.

Table 2. Conductance and Magnetic moment measurements.

Compounds	Conductance of respective complexes (in µs)	Magnetic moment (in B.M)
HBMB	-	-
MC1	97.3	0.0
MC2	00.0	3.18
MC3	00.0	1.91
MC4	00.0	0.0

3.1.2. UV -Visible spectroscopy.

Synthesized imine based ligand and its transition metal complexes were dissolved in DMSO and made with a micromolar solution. The above solutions were used to record the resultant ligand's UV-Visible spectra and its transition metal complexes. As depicted in Fig S1-S5, the peak appeared at 274 nm in the imine-based ligand due to the azomethine group, but in the case of complexes was shifted between 280 and 288 nm, indicating the involvement of azomethine in the coordinate bond formation. All the synthesized transition metal complexes exhibited a band between 397 and 405 nm due to the possibility of charge transfer transition [23]. The broadband located at 492 nm refers to the $^2B_{1g} \rightarrow {}^2E_g$ transitions; it recommends the complexes MC1 and MC2 belong to the distorted octahedral geometry [24].

3.1.3. FT-IR spectroscopy.

A band registers at 1646 cm^{-1} due to the free azomethine group of the HBMB ligand. However, the band was shifted to a lower wavenumber in the complexes suggesting its involvement in the coordination [25]. In the IR spectrum of ligand, a peak at 1432 cm^{-1} is due to the presence of stretching vibration of C=C group in the fused heterocyclic benzimidazole ring (Fig. S6-S10). In this part, representative IR spectrums of complexes MC1-MC4 are depicted and were compared with the synthesized ligand, HBMB. The shifting of these bands in the case of complexes strongly suggests that the imidazole ring nitrogen is attaching with the metal ion, and the bands appeared at 1683 and 14555 cm^{-1}. A medium band occurs at 1264 cm^{-1} due to the stretching vibration of a phenyl hydroxyl group in the imine based ligand, but the band is not located in the prepared complexes, indicating that the phenolic oxygen atom also acts as a donor site in the resultant complexes. The lower energy region of IR spectra exhibits bands occurring due to the M-N bond and M-O bond at 504 and 438 cm^{-1}.

3.1.4. Thermal studies.

All the obtained complexes from MC1 to MC4 have been subjected to read with thermogram over a broad range of temperature from 27 to 800 °C under inert atmosphere condition at 10 °C/min heating rate.

The thermal analysis of the complexes MC1 and MC2 is similar. The thermal degradation of the chemical substance in the MC2 complex is found in two stages. The initial step corresponding to the weight loss of lattice water molecule about 2.78% (calc. 2.617%) at a temperature range of 340-380 °C. Observable weight loss appeared in the next stage due to loss of two benzimidazole imine base ligand molecules; around weight loss occurs 87.59 % (calc. 82.52%) at temperature range appeared between 390 and 430 °C. Finally, at a temperature above 450 °C, the stable compound is left behind as metal oxide. The thermal action of the square planar complexes MC3 and MC4 are similar, while the decomposition is found in two phases. In the first phase, with reference to the loss of lattice water, about weight occurs 4.39% (calc. 4.27%) and the temperature region from 320 to 330 °C. Then, more significant weight loss refers to the decomposition of coordinated chloride and ligand (HBMD) at 430-470 °C, about the mass loss of 84.79% (calc. 75.81%).

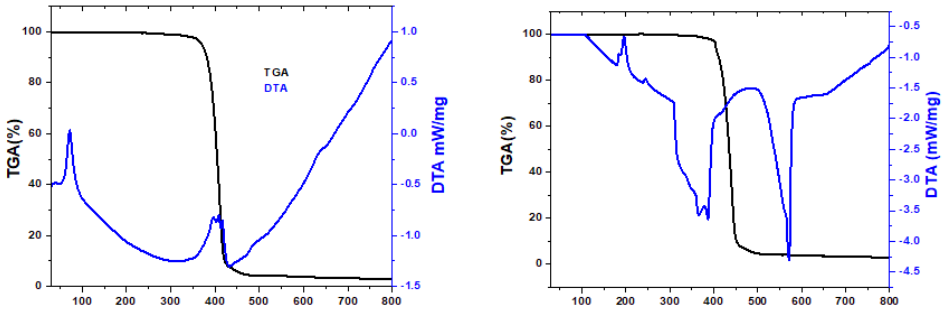

Figure 2. TGA and DTA for MC1 (left) and MC3 (right).

3.1.5. Mass spectral studies.

MC2 complex was concluded via MS technique the molecular ion peak appeared at m/z = 716.946, which is in complete agreement with its molecular weight; in the meanwhile, MC1 complex shows M+2 peak at m/z = 772.981 whereas molecular ion attributed at m/z = 770.986. The results clearly indicate that the complexes MC1 and MC2 are in a 1:2 (M: L) ratio. The complexes MC3 and MC4 are in the ratio 1:1 (M: L) were accepted from the molecular ion peak of MC3 complex registered at m/z = 446.9217 (theoretical value m/z = 446.170) whereas MC4 complex shows molecular ion peak at m/z = 577.9402 (theoretical value m/z = 577.7236) as shown in Fig (S12-S16).

3.1.6. ESR studies.

ESR spectra of polycrystalline compound MC3 were measured on X-band at a temperature of 77 K in DMSO solvent. The characteristic ESR spectra of copper complex MC3 are shown in Fig 3. Cu(II) complex containing one unpaired electron in its 3d orbital and effective spin S=1/2, which is equal to the free electron's actual spin with I= 3/2 for Cu^{2+}. The spectra of copper (II) complexes show four resolved peaks at the low-field region. The investigation of the spectrum gives $g_{\parallel}$ = 2.103 and $g_{\perp}$= 2.045; in addition to this information clearly indicates the trend $g_{\parallel} > g_{\perp} > 2.0022$, the manor also notice in the present study. The

studies indicate that the localization of unpaired electrons in Cu(II) ion dx^2-y^2 orbital is the actual spectral feature for axial symmetry. Tetragonal elongated geometry strongly recommends for the resultant MC3 complex [26].

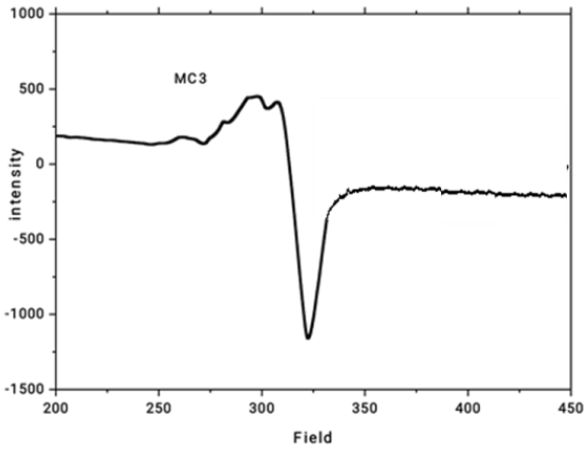

Figure 3. ESR spectrum of MC3 complex.

3.2. Biological activities.

3.2.1. Antimicrobial studies.

In the present investigation, *in vitro* antibacterial assay for the newly synthesized compounds were estimated against three Gram-positive bacteria such as *B. subtilis*, *L. monocytogenes*, and *S. aureus* and one gram-negative bacteria E. coli, in addition to this also studied in vitro antifungal activity by evaluating two fungi A. flavin and A. niger. A paramount range of zone of inhibition was visually examined around individual wells. The zone of inhibition around each well was quantified upon zone size in millimeters (mm). The quantified growths of inhibitions against both Gram-negative and Gram-positive microorganisms are listed in Table 3.

Table 3. Results of antimicrobial activity of MC1-MC4.

compounds	**Zone of inhibition (mm)[a]**					
	Bacteria				fungi	
	L. Monocytogenes	***B. subtilis***	***S. aureus***	***E. coli***	***A. niger***	***A. flavus***
HBMB	4	5	8	7	11	8
MC1	10	8	11	12	14	9
MC2	7	6	9	10	11	10
MC3	12	11	12	14	15	12
MC4	15	13	14	15	16	15
Ampicillin	23	24	25	27	-	-
Fluconazole	-	-	-	-	21	21

The results obtained are from the average of the three replicates.

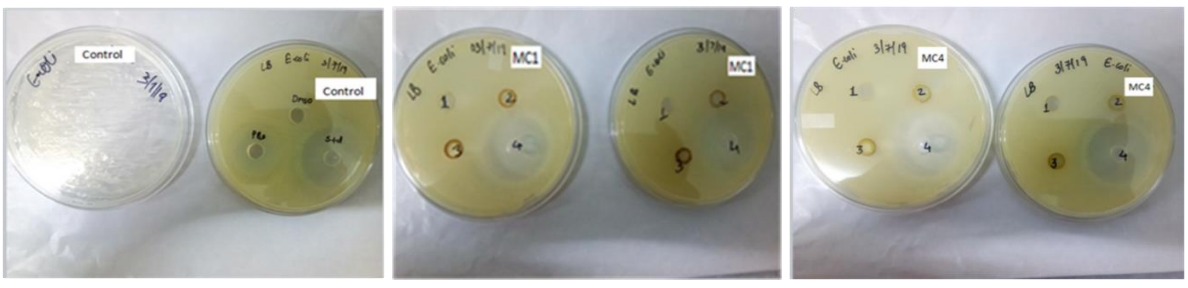

Figure 4. The bactericidal activity of MC1 and MC4 on *E. coli*.

3.2.2. Minimum inhibitory concentration (MIC).

To determine the minimum inhibitory concentration (MIC) value of resultant transition metal complexes (M1-M4) and the parent ligand, HBMB. The bacterial cultures were grown overnight; the concentration was adjusted and determined by the McFarland turbidity standard. The serial dilution method was carried out to investigate the MIC of HBMB and MC1-MC4 in microtitre plate assay. All the synthesized compounds show a significant range of MIC against resultant Gram-positive as well as Gram-negative bacteria Table 4. Among the synthesized complexes, the complex MC4 showed significant antimicrobial activity due to halogen ion presence inside the coordination sphere. The Overtone concept of cell permeability clearly reveals the high activity of the compounds [27]. The cell, surrounded by a lipid layer the cell, allows only soluble compounds to pass through it. The obtained results are strongly suggested that the synthesized compounds can be used in the resistant bacterial treatment towards the novel antimicrobial drug development.

Table 4. Minimum inhibitory concentration results of ligand and complexes.

Range of concentration (µg/mL)[a]

compounds	Bacteria				Fungi	
	L. Monocytogenes	***B. subtilis***	***S. aureus***	***E. coli***	***A. niger***	***A. Flavus***
HBMB	98	97	99	98	91	92
MC1	93	95	94	97	83	89
MC2	96	96	97	96	86	84
MC3	95	90	91	96	88	87
MC4	91	90	90	94	82	80
Ampicillin	26	29	26	27	-	-
Fluconazole	-	-	-	-	43	43

The results obtained are from the average of the three replicates.

3.2.3. Antioxidant results: DPPH –scavenging activity.

The DPPH assay was used to perform the free radical scavenging activity of newly synthesized compounds. In the DPPH assay, the capable of the scrutinized resultant compound to act as electron transfer or hydrogen donor in the conversion of DPPH radical from radical form to reduced form DPPH-H was analyzed. The compound's ability to energetically scavenge DPPH radical, that was investigated, and it is compared with that of standard ascorbic acid. A color change from a deep purple (DPPH radical) into a yellow color (DPPH-H) in the reaction mixture suggests its antioxidant activity. Its efficacy was estimated by measuring the absorbance at 517 nm. A high free radical scavenging activity was confirmed by the lower absorbance value of the reaction mixture. The IC_{50} value of the compounds HBMB and MC1-MC4 were comparable to standard ascorbic acid. However, the compound MC4 exhibits the highest activity and lowest for MC2 with the parent ligand HBMB. Following the order MC4>MC3>MC1>MC2>HBMB, the highest activity register for MC4 due to the presence of halogen present in the platinum complex's coordination sphere. Several investigations recommend that halogens' presence increases the cellular antioxidant activity by enhancing lipophilicity and cell membrane solubility of a drug [28, 29]. Therefore, the least value attributed for MC2 is due to the without halogen in the coordination. Table 5 represents the IC_{50} value of synthesized compounds.

Table 5. Antioxidant ability (IC_{50}) of all the synthesized compounds.

Compounds	IC_{50} (µg/mL) ± S.D*
AA	24±0.55
HBMB	75±0.43
MC1	75±0.23
MC2	91±0.45
MC3	70±0.85
MC4	63±0.29

AA= Ascorbic acid

*S.D= Standard deviation (average of three replicates)

3.2.4. BSA binding interaction

3.2.4.1. UV-titration studies.

The protein's structural changes were explored by using electronic absorption spectra and investigated the binding interaction between protein (BSA) and complexes (MC1-MC4). The UV-Visible absorption spectra of BSA were performed *with* and without metal complexes (MC1 and MC4), as shown in Fig 5. In this study, a characteristic spectrum of complexes (MC1 and MC4) are taken to exhibit binding of complexes with BSA, the strong absorption band at 231 nm shows the characteristic of alpha-helix arrangement in a framework confirmation of the of polypeptide protein skeleton and other broad peak occurs at 284 nm is due to the aromatic ring in the amino acids (Phe, Tyr, Trp) [30, 31]. And successive addition of MC1-MC4 to protein (BSA) solution, the intensity of the BSA peak at 231 nm increased with 2 nm red shift occurs, and the maximum absorption band intensity at 284 nm is decreased with no such considerable change. The isosbestic point appears at 295nm, where complexes: BSA has the same intensity of absorption. It is equilibrium inductive between bound complexes and the free form of the complexes. The band attributed at 295 nm for unbounded BSA which enhanced with successive addition of complex compound, recommends that the bounded with BSA energetically by the aggregation of BSA induces intensified in absorption at high concentration of complexes in that particular region and the change in the absorption spectra of the fluorophore induce the static quenching procedure followed. These results can be described by the interaction of BSA with MC1-MC4, which causes the protein-peptide strands were unfolding and loosening and the hydrophobicity of the BSA microenvironment was altered [32].

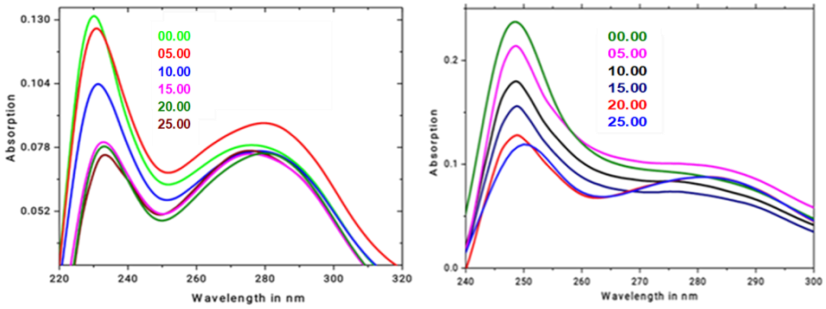

Figure 5. Absorption spectra of the complexes {MC1 (Left) and MC4 (Right)} with different concentration of BSA; [MC1 and MC4] = 25.00 µM and [BSA] = 00.00-25.00µM at room temperature. The change in absorbance upon increasing concentration of BSA.

3.2.4.2. Fluorescence titration.

The fluorescence emission studies fit to investigate the binding character of complexes with BSA as shown in Fig 6. The peak appears at 382 nm due to the strong fluorescence

emission spectra of BSA. It was probably that the examined fluorescence intensity of BSA effectively decreased with the gradual addition of complexes concentration and followed by a redshift reveals that the existence of some binding interaction between complexes (MC1-MC4) and BSA, accordingly quenching the intrinsic fluorescence of BSA and change the microenvironment of the fluorophore. The quenching of fluoresce mechanism was studied by Stern-Volmer equation (2):

$$Fo/F = 1+ K_{Sv} [Q] =1+ K_q \tau o [Q] \qquad (2)$$

Where, F_o and F are the fluorescence intensities of BSA with and without complexes (MC1-MC4), respectively. K_q and [Q] are the constant of bimolecular quenching concentration of quencher, respectively. τ_o is the fluorophore lifetime in the absence of quencher ($\tau_o = 10^{-8}$ s) and the Stern-Volmer quenching constant. It is calculated by using the slope of linear regression plot F_o/F v/s [Q].

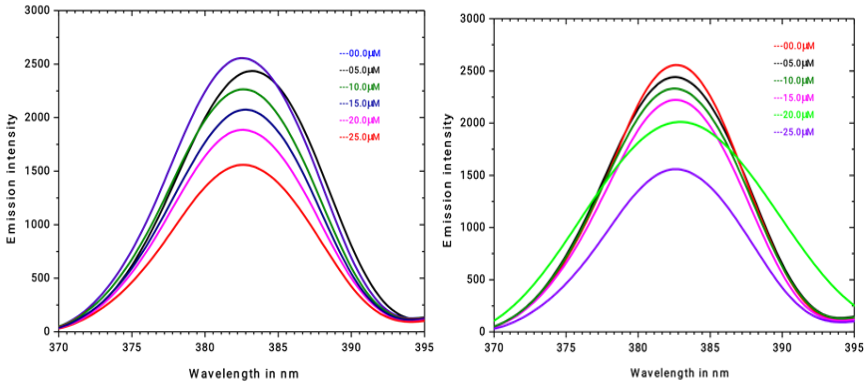

Figure 6. Fluorescence emission spectra of BSA in the presence of various concentration of complexes {MC1 (left) and MC4 (Right)}; [BSA] = 10×10^{-6}M; [MC1 and MC4] = 00.00-25.00 µM at 05.00 µM increment.

The fluorescence quenching of BSA tryptophan residues of fluorescence quenching by complex MC4 at three different temperatures is depicted in Fig. 7. The K_{SV} and K_q are the binding interaction of complexes MC1-MC4 with BSA (Table 6). Results recommend a good BSA binding efficacy for MC4 compare to all other prepared complexes. The values of K_q obtained are in the order of (10^{-13} $M^{-1}s^{-1}$), which are greater than various quenchers for fluorescence of biopolymer described (2×10^{-10} $M^{-1}s^{-1}$), representing the presence of a static quenching mechanism (equation 3) [33, 34].

$$\log [F_o\text{-}F/F] = \log K_{bin} + n \log [Q] \qquad (3)$$

The results exhibit the quenching constant K_{SV} of the Stern-Volmer is inversely connected with temperature. It confirms that the probable mechanism of single fluorescence quenching of BSA by MC1-MC4 is started by a static quenching process via compound formation rather than energetic collision, as it depends on dispersion. In contradiction, increased temperature affects the complexes' decreased stability between the BSA and synthesized metal complexes. Thus the static quenching constant exhibits a lower value [35].

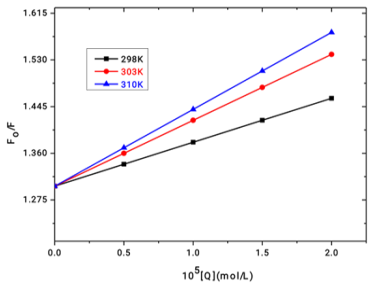

Figure 7. Ster-Volmer plot at different temperatures.

Table 6. The quenching parameter for BSA-complexes at different temperatures.

Complexes	T (K)	$K_{sv} \times 10^{-5}$ ($Lmol^{-1}$)	$K_q \times 10^{13}$ ($Lmol^{-1}s^{-1}$)	R^2 (correlation coefficient)
MC1	298	1.739	1.970	0.9319
	303	1.618	1.862	0.9092
	310	1.478	1.810	0.9014
MC2	298	1.795	2.127	0.9432
	303	1.634	2.001	0.9305
	310	1.577	1.997	0.9195
MC3	298	2.123	2.247	0.9713
	303	1.805	2.015	0.9611
	310	1.745	1.969	0.9281
MC4	298	2.971	2.577	0.9803
	303	2.454	2.133	0.9780
	310	2.076	1.887	0.9690

3.2.4.3. Binding parameters.

The equilibria of binding analysis were investigated using the intensity of fluorescence data and a double-logarithmic regression curve with the equation (3) [36]. In which the F_O and F are the fluorescence intensity of BSA with and without metal complexes [Q], respectively. The binding constant between complexes and BSA was represented by K_b and the average number of binding sites per albumin. The slop and intercept were used to calculate the value of n and K_b, respectively, by constructing the graph log [F/ (F_o- F) vs. log [Q] (intercept= K_b) as depicted in Fig. 8, and the reduction of the complex formation stability between the BSA and prepared compounds (MC1-MC4) were confirmed by the value of K_b is formed to decreased considerably with increasing temperature because due to the exothermic nature of bonding nature process at high temperature. The magnitude of the K_b value of complexes MC1-MC4 was listed in Table 7 [37] and indicating the strong binding of complexes with BSA. Among all the prepared complexes, the complex MC4 was good binding activity due to halogen presence in the coordination sphere of the platinum complex. Decreased value of n with increasing in the temperature as good agreement to the interaction's exothermic behavior and the value all most equal to ~1 indicate that the complexes binding with BSA according to the 1:1 mole ratio which trend recommends the presence of the single binding site.

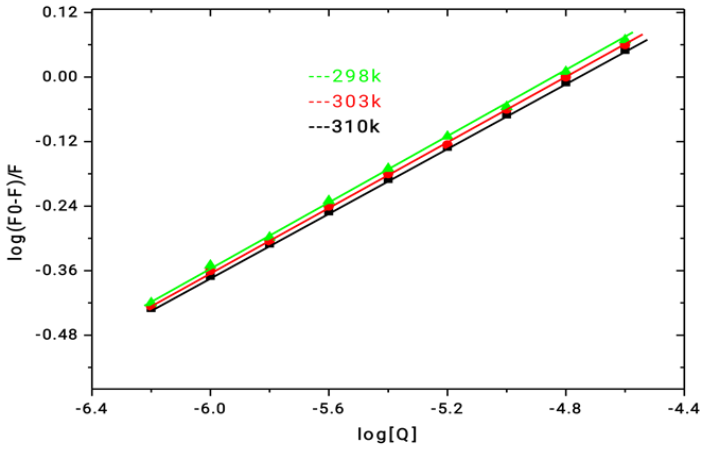

Figure 8. Double-log plots of MC4 changing effect on BSA (30 µM) at different temperatures. The concentration of MC4 from 0 to 25 µM was 00.00 05.00, 10.00, 15.00, 20.00 and 25.00 µM.

The thermodynamic parameters were calculated to elucidate the binding interaction between complexes (MC1-MC4) and BSA. The acting force of binding character occurs between complexes and biomolecules such as van der-Waals forces, electrostatic forces, hydrogen bonds, and hydrophobic interaction forces. The free energy (ΔG°), enthalpy (ΔH°),

and entropy (ΔS°) are the thermodynamic parameters that were used to determine the binding mode of the reaction between complexes and BSA [38, 39]. The temperatures were select at 298, 303, and 310 K, and thus structure degradation of BSA will not occur as well as; when there is no considerable change in temperature, the enthalpy of the reaction can be treated as constant, and further its value can be determined from equation (4) and (5) [33, 37].

$$\log K_b = -\frac{\Delta H°}{2.303RT} - \frac{\Delta S°}{2.303R} \quad (4)$$

$$\Delta G° = \Delta H° - T\Delta S° = -RT \ln K_{bin} \quad (5)$$

where K_b is the binding constant at the particular temperature, R is the gas constant, and the temperature is denoted by T.

In accordance with the obtained binding constant K_b of MC1-MC4 with BSA at the investigated temperatures, the thermodynamic parameters have been estimated from the Van't Hoff equation took by a linear plot as observed in Fig 9. Table 7 register the relative thermodynamic parameters and the BSA binding constant. It is indicated that the change in Gibbs free energy (ΔG°) recommends that the binding reaction's spontaneity between complexes and BSA increases with an increasing temperature range from 298 to 310K. The negative value of ΔH° and ΔS° suggests that either van der Waals forces or hydrogen bonds play a significant role in the binding mechanism and is nature exhibit the exothermic character. The formation of the system is entropy-driven at T ΔS°> ΔH°.

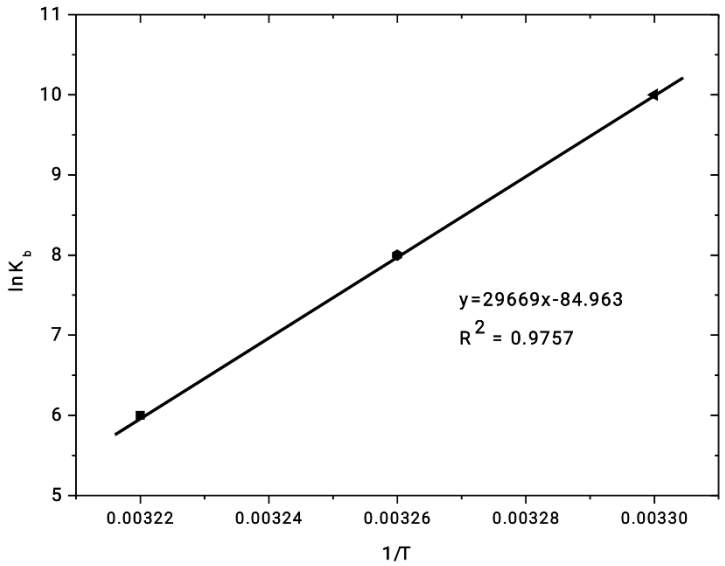

Figure 9. Van't Hoff plot of **MC4**-BSA system.

Table 7. The binding constant of the relative thermodynamic parameter for the BSA-complex system at different temperatures.

Compound	T (K)	$K_b \times 10^5$ ($Lmol^{-1}$)	N	R^2	ΔG° ($kJmol^{-1}$)	ΔH° ($kJmol^{-1}$)	ΔS° ($JK^{-1}mol^{-1}$)
MC1	298	4.21	0.81	0.9819	-24.978		
	303	3.29	0.79	0.9810	-24.591	-47.311	-95.23
	310	2.14	0.75	0.9801	-24.121		
MC2	298	4.09	0.80	0.9803	-24.129		
	303	3.91	0.72	0.9734	-24.055	-45.985	-94.10
	310	2.67	0.70	0.9699	-24.129		
MC3	298	4.12	0.83	0.9939	-25.396		
	303	3.45	0.81	0.9912	-25.119	-51.245	-96.09
	310	2.01	0.78	0.9903	-24.496		
MC4	298	5.11	0.88	0.9985	-26.669		
	303	4.81	0.82	0.9938	-26.298	-55.344	-97.67
	310	3.57	0.73	0.9903	-25.423		

3.2.4.4. Energy transfer between BSA and MC1-MC4.

The distance between an acceptor and a donor molecule can be measured using a non-destructive spectroscopic technique of Forster non-radioactive energy transfer (FRET). The dipole-dipole interaction exists between an excited donor species, and an acceptor causes the FRET. The energy transfer efficiency is based on the sixth inverse power of the separation distance between the acceptor and a donor.

To confirm BSA analogs' circumference [40, 41], the fluorescence resonance energy transfer (FRET) BSA to complexes MC1-MC4 was verified. Agreeing to the Forster hypothesis of non-radioactive energy transfer, the transfer of energy takes place through a direct electrodynamic interaction between a primary energized molecule and its neighbor. The following equation (6) can be used to calculate the (FRTE) where r is the critical transfer distance between the complexes and BSA.

$$E = 1 - \frac{R_0^6}{R_0^6 + r^2} \qquad (6)$$

The energy transfer efficiency between a donor and an acceptor is denoted by E. F, and F_0 are fluorescence intensities of BSA with and without quencher, respectively. R_0, represents the critical energy transfer distance (Forster distance) when the transfer efficiency is exactly half and given by the below equation (7).

$$R_0^6 = 8.79k^2N^{-4}J\varphi N^{-4} \qquad (7)$$

where k is the donor and acceptor dipoles orientation factor, the refractive index of the medium is denoted by N, ψ is the quantum yield of fluorescence of the donor in the presence of acceptor, the degree of spectral overlap between the emission of donor and the absorption of acceptor and expressed by J (equation 8).

$$J = \frac{\Sigma F(\lambda)\varepsilon(\lambda)\lambda^4\, d\lambda}{\Sigma F(\lambda)d\lambda} \qquad (8)$$

where F (λ) is the intensity of the fluorescence emission of the donor in the range of wavelength, and ε(λ)is the acceptor molar absorption coefficient. In accordance with equations 6-8 and employing a spatial orientation factor of the dipole k^2= 2/3, with the refractive index of the medium (N) =1.336 and φ = 0.15. J, R_0, r, and E were listed in Table 8. On successive addition of complexes, the fluorescence intensity of the tryptophan's residue present in the BSA decreased with a complimentary increase in the intensity of fluorescence at the range of 370 nm and 390 nm (Fig. 6).

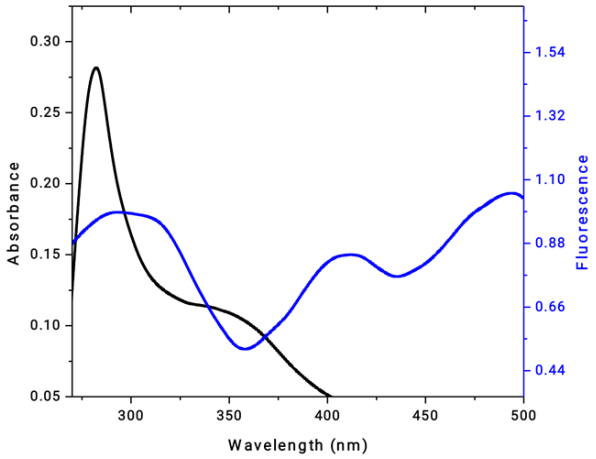

Figure 10. Spectral overlap of the absorption of **MC4** (black curve) and the fluorescence spectrum of BSA (blue curve).

This attributes a capable energy exchange from the tryptophan residue (Trp-134) in BSA to the complexes. The absorption spectrum of the complexes was overlapped with the BSA emission spectra are observed in Fig. 10. It has been visually examined as the distance (r) and the Trp residue (as a residue) and acceptor. The value of r more significant compared with that of R_0, one more indication of a static quenching mechanism in binding interaction between the complexes and BSA [42, 43].

Table 8. Distance parameter of BSA with complexes MC1-MC4.

Compound	J (cm^3Lmol^{-1})	E(%)	R_0(nm)	r(nm)
MC1	2.1×10^{-14}	0.071	3.01	3.17
MC2	2.0×10^{-14}	0.069	3.03	3.13
MC3	2.3×10^{-14}	0.073	2.97	3.21
MC4	2.4×10^{-14}	0.075	2.88	3.23

4. Conclusions

The fused heterocyclic Schiff base ligand, 2-{(E)-[(1H-benzimidazol-2-ylmethyl)imino]methyl}-4-bromophenol (HBMB) was synthesized and elucidated by various spectroscopic techniques such as NMR, IR, Mass, and UV followed by preparation of Co(III), Ni(II), Cu(II) and Pt(II) transition metal complexes. The stoichiometry ratio between the transition metal and the ligand of these resultant complexes is 1:2 (M:L) and 1:1 (M:L) and structurally elucidated them with the help of spectroscopic techniques as well as conductance measurement. Based on the obtained spectroscopic data, an octahedral environment around the Co(III) and Ni(II) complexes and a square planar environment around the Cu(II) and Pt(II) complexes have been proposed. All the prepared compounds were screened for *in vitro* antimicrobial studies against selected bacterial and fungal strains. The complexes exhibit a good binding affinity to BSA protein giving comparatively appreciable binding constants. The fluorescence studies found that the complex is a greater quencher and interacts with BSA via a static quenching mechanism, which further exerts that the temperature increases with decreasing K_{sv}. The results also exhibited that the values of ΔH^o, $\Delta S^{o,}$ and ΔG^o are negative. It can be concluded that the main force between BSA and the transition metal complexes are the hydrophobic force. This study's biological importance is evident since serum albumin could act as a carrier protein for these complexes.

Funding

This research received no external funding.

Acknowledgments

The authors are sincerely thankful to IIT Mumbai and IOE, University of Mysore, for their kind cooperation in metal complexes' characterization. SPK thank the Director, Amrita Vishwa Vidyapeetham, Mysuru Campus, for providing the necessary support.

Conflicts of Interest

The authors declare no conflict of interest.

References

1. Ali Mohd, G.; Ayaz Mahmood, D.; Fairooz Ahmad, K.; Bashir Ahmad, D. Benzimidazole Derivatives as Potential Antimicrobial and Antiulcer Agents: A Mini Review. *Mini-Reviews in Medicinal Chemistry* **2019**, *19*, 1292-1297, https://doi.org/10.2174/1381612824666181017102930.
2. Prasad, K.S.; Pillai, R.R.; Armaković, S.; Armaković, S.J. Photophysical properties and theoretical investigations of newly synthesized pyrene-naphthalene based Schiff base ligand and its copper(II) complexes. *Inorganica Chimica Acta* **2019**, *486*, 698-703, https://doi.org/10.1016/j.ica.2018.11.045.
3. Suk, F.-M.; Liu, C.-L.; Hsu, M.-H.; Chuang, Y.-T.; Wang, J.P.; Liao, Y.-J. Treatment with a new benzimidazole derivative bearing a pyrrolidine side chain overcomes sorafenib resistance in hepatocellular carcinoma. *Scientific Reports* **2019**, *9*, 1-10, https://doi.org/10.1038/s41598-019-53863-2.
4. Kollur, S.P.; Castro, J.O.; Frau, J.; Flores-Holgu´ın, N.; Shruthi, G.; Shivamallu, C.; Glossman-Mitnik, D. Preparation, spectroscopic investigations and chemical reactivity properties of a new schiff base ligand and its copper (II) complexes. *Journal of Molecular Structure* **2019**, *1191*, 17-23, https://doi.org/10.1016/j.molstruc.2019.03.101.
5. Carreira, M.; Calvo-Sanjuán, R.; Sanaú, M.; Zhao, X.; Magliozzo, R.S.; Marzo, I.; Contel, M. Cytotoxic hydrophilic iminophosphorane coordination compounds of d8 metals. Studies of their interactions with DNA and HSA. *Journal of Inorganic Biochemistry* **2012**, *116*, 204-214, https://doi.org/10.1016/j.jinorgbio.2012.06.017.
6. Panchsheela Ashok, U.; Prasad Kollur, S.; Prakash Arun, B.; Sanjay, C.; Shrikrishna Suresh, K.; Anil, N.; Vasant Baburao, H.; Markad, D.; Ortega Castro, J.; Frau, J.; Flores-Holguín, N.; Glossman-Mitnik, D. In vitro anticancer activity of 4(3H)-quinazolinone derived Schiff base and its Cu(II), Zn(II) and Cd(II) complexes: Preparation, X-ray structural, spectral characterization and theoretical investigations. *Inorganica Chimica Acta* **2020**, *511*, 1-32, https://doi.org/10.1016/j.ica.2020.119846.
7. Skyrianou, K.C.; Psycharis, V.; Raptopoulou, C.P.; Kessissoglou, D.P.; Psomas, G. Nickel–quinolones interaction. Part 4 — Structure and biological evaluation of nickel(II)–enrofloxacin complexes compared to zinc(II) analogues. *Journal of Inorganic Biochemistry* **2011**, *105*, 63-74, https://doi.org/10.1016/j.jinorgbio.2010.09.007.
8. Jin, Y.; Lewis, M.A.; Gokhale, N.H.; Long, E.C.; Cowan, J.A. Influence of Stereochemistry and Redox Potentials on the Single- and Double-Strand DNA Cleavage Efficiency of Cu(II)· and Ni(II)·Lys-Gly-His-Derived ATCUN Metallopeptides. *Journal of the American Chemical Society* **2007**, *129*, 8353-8361, https://doi.org/10.1021/ja0705083.
9. Prasad, K.S.; Shruthi, G.; Shivamallu, C. Synthesis, characterization, in silico analysis and physicochemical properties of tin(II) and lead(II) coordination complexes prepared using 2-((3,5-dimethoxybenzylidene)amino)pyridin-3-ol and 1,10-phenanthroline. *Polyhedron* **2019**, *157*, 536-547, https://doi.org/10.1016/j.poly.2018.10.037.
10. Mahesh, S.V.; Manoj, N.B.; Sanjay, K.R.; Divya, J.J.; Prachi, T.A.; Dhaval, B.P.; Hitesh, D.P. Benzimidazole: A Milestone in the Field of Medicinal Chemistry. *Mini-Reviews in Medicinal Chemistry* **2020**, *20*, 532-565, https://doi.org/10.2174/1389557519666191122125453.
11. Sunil, K.N.; Krishnamurthy, G.; Yadav, D.B.; Vikas, H.M.; Ravikumar, N.T.R.; Shivananda, K.; Prabhakar, B.T. Synthesis, characterization and tumor inhibitory activity of a novel Pd(II) complex derived from methanethiol-bridged (2-((1H-benzo[d]imidazol2-yl)methylthio)-1H-benzo[d]imidazol6-yl)(phenyl)methanone. *New J. Chem* **2019**, *43*,790-806, https://doi.org/10.1039/c8nj03057j.
12. Dash, S.P.; Panda, A.K.; Dhaka, S.; Pasayat, S.; Biswas, A.; Maurya, M.R.; Majhi, P.K.; Crochet, A.; Dinda, R. A study of DNA/BSA interaction and catalytic potential of oxidovanadium(v) complexes with ONO donor ligands. *Dalton Transactions* **2016**, *45*, 18292-18307, https://doi.org/10.1039/C6DT03228A.
13. Ibrahim, H.A.; Refaat, H.M. Versatile mechanisms of 2-substituted benzimidazoles in targeted cancer therapy. *Future Journal of Pharmaceutical Sciences* **2020**, *6*, 1-20, https://doi.org/10.1186/s43094-020-00048-8.
14. Tahmasbi, L.; Sedaghat, T.; Motamedi, H.; Kooti, M. Mesoporous silica nanoparticles supported copper(II) and nickel(II) Schiff base complexes: Synthesis, characterization, antibacterial activity and enzyme immobilization. *Journal of Solid State Chemistry* **2018**, *258*, 517-525, https://doi.org/10.1016/j.jssc.2017.11.015.
15. Maurya, R.C.; Chourasia, J.; Rajak, D.; Malik, B.A.; Mir, J.M.; Jain, N.; Batalia, S. Oxovanadium(IV) complexes of bioinorganic and medicinal relevance: Synthesis, characterization and 3D molecular modeling of some oxovanadium(IV) complexes involving O, N-donor environment of salicylaldehyde-based sulfa drug Schiff bases. *Arabian Journal of Chemistry* **2016**, *9*, S1084-S1100, https://doi.org/10.1016/j.arabjc.2011.12.012.
16. Prakasha, G.; Shiva, P.K.; Syed, I.; Hosakere, D.R. Novel Benzimidazole Derived Imine-Based Ligand and its Co (III), Ni(II), Cu(II) and Pt(II) Complexes: Chemical Synthesis, Structure, Antimicrobial, DNA Interaction Studies and Nuclease Activity. *Letters in applied nanobioscience* **2020,** *9*, 1655–1672**,** https://doi.org/10.33263/LIANBS94.16551672.

17. Yogita, B.; Manjinder, K.; Gulshan, B. Antimicrobial Potential of Benzimidazole Derived Molecules. *Mini-Reviews in Medicinal Chemistry* **2019**, *19*, 624-646, http://dx.doi.org/10.2174/1389557517666171101104024.
18. Abdel-Motaal, M.; Almohawes, K.; Tantawy, M.A. Antimicrobial evaluation and docking study of some new substituted benzimidazole-2yl derivatives. *Bioorganic Chemistry* **2020**, *101*, https://doi.org/10.1016/j.bioorg.2020.103972.
19. Ommenya, F.K.; Nyawade, E.A.; Andala, D.M.; Kinyua, J. Synthesis, Characterization and Antibacterial Activity of Schiff Base, 4-Chloro-2-{(E)-[(4-Fluorophenyl)imino]methyl}phenol Metal (II) Complexes. *Journal of Chemistry* **2020**, *2020*, 1-8, https://doi.org/10.1155/2020/1745236.
20. Blois, M.S. Antioxidant Determinations by the Use of a Stable Free Radical. *Nature* **1958,** *181*, 1199-1200, https://doi.org/10.1038/1811199a0.
21. Disha, S.; Hosakere, D.R.; Basappa, C.V.K.; Basavegowda, J.; Nangappagowda, D.R. Co(III) and VO(IV) complexes with a new bidentate Schiff base: Interaction with BSA and antimicrobial studies. *Biointerface Research in Applied Chemistry* **2019**, *9*, 3776 – 3782, https://doi.org/10.33263/BRIAC91.776782.
22. Jha, N.N.; Ray, I.P. Magnetic studies on Co(II) and Ni(II) complexes of hydroxamic acid. *Asian Journal of Chemistry* **2000**, *12*, 703-706.
23. Shakya, R.; Imbert, C.; Hratchian, H.P.; Lanznaster, M.; Heeg, M.J.; McGarvey, B.R.; Allard, M.; Schlegel, H.B.; Verani, C.N. Structural, spectroscopic, and electrochemical behavior of trans-phenolato cobalt(iii) complexes of asymmetric NN′O ligands as archetypes for metallomesogens. *Dalton Transactions* **2006**, *21*, 2517-2525, https://doi.org/10.1039/B514190G.
24. Raman, N.; Ravichandran, S.; Thangaraja, C. Copper(II), cobalt(II), nickel(II) and zinc(II) complexes of Schiff base derived from benzil-2,4-dinitrophenylhydrazone with aniline. *Journal of Chemical Sciences* **2004**, *116*, 215-219, https://doi.org/10.1007/BF02708270.
25. Ommenya, F.K.; Nyawade, E.A.; Andala, D.M.; Kinyua, J. Synthesis, Characterization and Antibacterial Activity of Schiff Base, 4-Chloro-2-{(E)-[(4-Fluorophenyl)imino]methyl}phenol Metal (II) Complexes. *Journal of Chemistry* **2020**, *2020*, https://doi.org/10.1155/2020/1745236.
26. Kivelson, D.; Neiman, R. ESR Studies on the Bonding in Copper Complexes. *The journal of chemical physics* **1961**, *149*, 1-8, https://doi.org/10.1063/1.1731880.
27. Dharmaraja, J.; Subbaraj, P.; Esakkidurai, T.; Shobana, S. Studies on Ni(II), Cu(II) and Zn(II) complexes with 2-aminobenzamide and some bioactive imidazole enzyme constituents. *Journal of Coordination Chemistry* **2015**, *68*, 4314-4344, https://doi.org/10.1080/00958972.2015.1101758.
28. Gentry, C.L.; Egleton, R. D.; Gillespie, T.; Abbruscato, T. J.; Bechowski, H. B.; Hruby, V. J.; Davis, T. P. Modifying peptide properties by prodrug design for enhanced transport into the CNS. *Peptides* **1999**, *20*, 1229-1238, https://doi.org/10.1007/978-3-0348-8049-7_6.
29. Amine, O.; Fatiha, M.; Asmae, L.; Souad, H.; Mohammed, B.; Noureddine, K. DPPH scavenging activity of some Bis-benzimidazole derivatives. *Mediterranean Journal of Chemistry* **2019**, *8*, 103-107, https://doi.org/10.13171/10.13171/mjc8219041101ao.
30. Karami, K.; Hosseini-Kharat, M.; Sadeghi-aliabadi, H. In vitro cytotoxicity studies of palladacyclic complexes containing the symmetric diphosphine bridging ligand; Studies of their interactions with DNA and BSA. *European Journal of Medicinal Chemistry* **2014**, *73*, 8-17, https://doi.org/10.1016/j.ejmech.2013.11.042.
31. Sanatkar, T.H.; Hadadzadeh, H.; Jannesari, Z.; Khayamian, T.; Ebrahimi, M.; Rudbari, H.A.; Torkzadeh-Mahani, M.; Anjomshoa, M. Characterization, photocleavage, molecular modeling, and DNA- and BSA-binding studies of Cu(II) and Ni(II) complexes with the non-steroidal anti-inflammatory drug meloxicam. *Inorganica Chimica Acta* **2014**, *423*, 256-272, https://doi.org/10.1016/j.ica.2014.08.060.
32. Sharma, D.; Revanasiddappa, H.D.; Jayalakshmi, B. DNA binding, BSA interaction and in-vitro antimicrobial studies of Cu(II), Co(III), Ni(II) and VO(IV) complexes with a new Schiff base. *Egyptian Journal of Basic and Applied Sciences* **2020**, *7*, 323-341, https://doi.org/10.1080/2314808X.2020.1758890.
33. Asadpour, S.; Aramesh-Boroujeni, Z.; Jahani, S. In vitro anticancer activity of parent and nano-encapsulated samarium(iii) complex towards antimicrobial activity studies and FS-DNA/BSA binding affinity. *RSC Advances* **2020**, *10*, 31979-31990, https://doi.org/10.1039/d0ra05280a.
34. Meti, M.D.; Nandibewoor, S.T.; Joshi, S.D.; More, U.A.; Chimatadar, S.A. Multi-spectroscopic investigation of the binding interaction of fosfomycin with bovine serum albumin. *Journal of Pharmaceutical Analysis* **2015**, *5*, 249-255, https://doi.org/10.1016/j.jpha.2015.01.004.
35. Bou-Abdallah, F.; Sprague, S.E.; Smith, B.M.; Giffune, T.R. Binding thermodynamics of Diclofenac and Naproxen with human and bovine serum albumins: A calorimetric and spectroscopic study. *The Journal of Chemical Thermodynamics* **2016**, *103*, 299-309, https://doi.org/10.1016/j.jct.2016.08.020.
36. Chakraborty, G.; Ray, A.K.; Singh, P.K.; Pal, H. Non-covalent interaction of BODIPY-benzimidazole conjugate with bovine serum albumin–A photophysical and molecular docking study. *Journal of Photochemistry and Photobiology A: Chemistry* **2019**, *377*, 220-227, https://doi.org/10.1016/j.jphotochem.2019.04.001.

37. Wei, Y.-L.; Li, J.-Q.; Dong, C.; Shuang, S.-M.; Liu, D.-S.; Huie, C.W. Investigation of the association behaviors between biliverdin and bovine serum albumin by fluorescence spectroscopy. *Talanta* **2006**, *70*, 377-382, https://doi.org/10.1016/j.talanta.2006.02.052.
38. Zhang, Y.; Xiang, X.; Mei, P.; Dai, J.; Zhang, L.; Liu, Y. Spectroscopic studies on the interaction of Congo red with bovine serum albumin. *Spectrochimica. Acta, Part A* **2009**, *72*, 907-914, https://doi.org/10.1016/j.saa.2008.12.007.
39. Li, Y.; Yang, G.; Mei, Z. Spectroscopic and dynamic light scattering studies of the interaction between pterodontic acid and bovine serum albumin. *Acta Pharmaceutica Sinica B* **2012**, *2*, 53-59, https://doi.org/10.1016/j.apsb.2011.12.001.
40. Ross, P.D.; Subramanian, S. Thermodynamics of protein association reactions: forces contributing to stability. *Biochemistry* **1981,** *20*, 3096-3102, https://doi.org/10.1021/bi00514a017.
41. Singla, P.; Luxami, V.; Paul, K. Synthesis and in vitro evaluation of novel triazine analogues as anticancer agents and their interaction studies with bovine serum albumin. *European Journal of Medicinal Chemistry* **2016**, *117*, 59-69, https://doi.org/10.1016/j.ejmech.2016.03.088.
42. Jannesari, Z.; Hadadzadeh, H.; Khayamian, T.; Maleki, B. Experimental and molecular modeling studies on the interaction of the Ru(II) -piroxicam with DNA and BSA. *European Journal of Medicinal Chemistry* **2013**, *69*, 577-590, https://doi.org/10.1016/j.ejmech.2013.08.051.
43. Singh, I.; Luxami, V.; Paul, K. Synthesis, cytotoxicity, pharmacokinetic profile, binding with DNA and BSA of new imidazo[1,2-a]pyrazine-benzo[d]imidazol-5-yl hybrids. *Scientific Reports* **2020**, *10*, 1-14, https://doi.org/10.1038/s41598-020-63605-4.

Supporting information

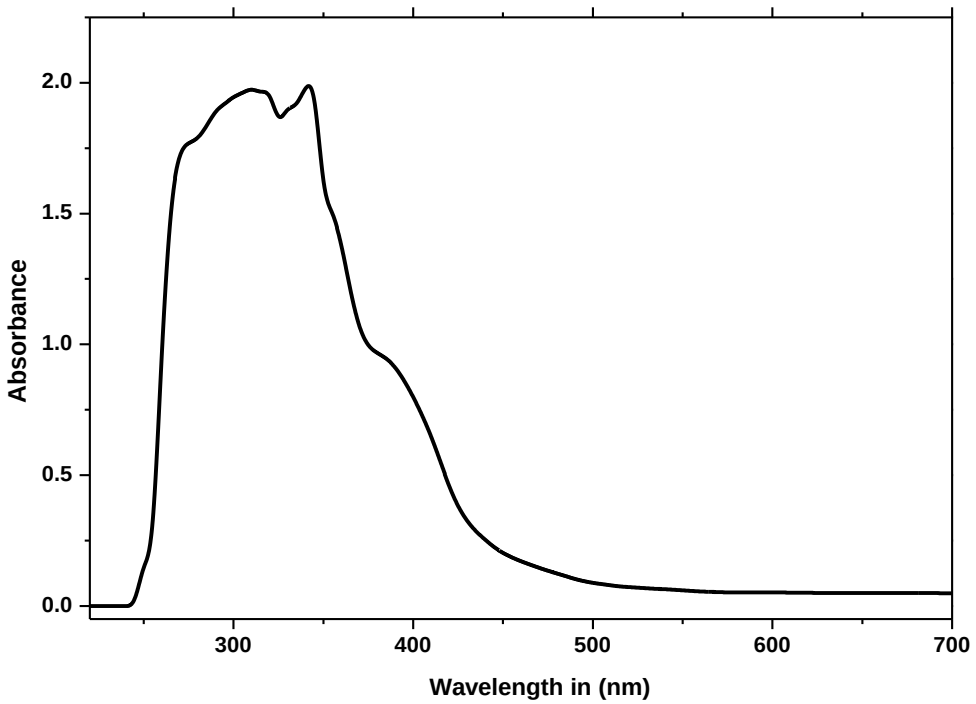

Figure S1. UV-visible spectra of compound HBMB.

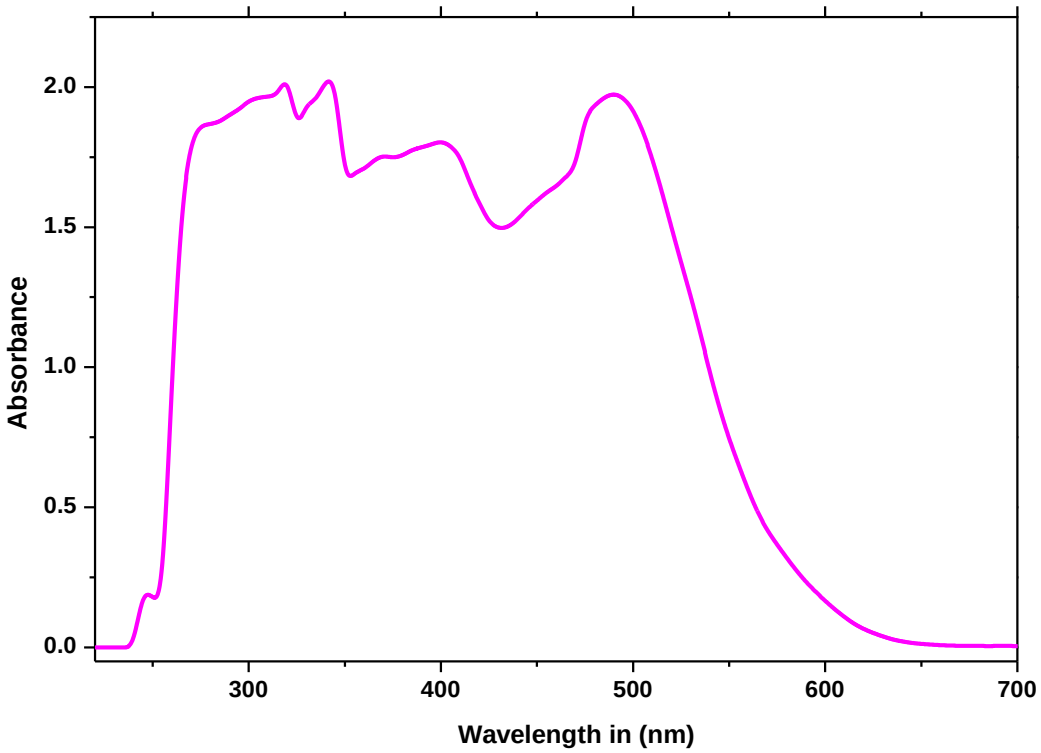

Figure S2. UV-visible spectra of compound MC1.

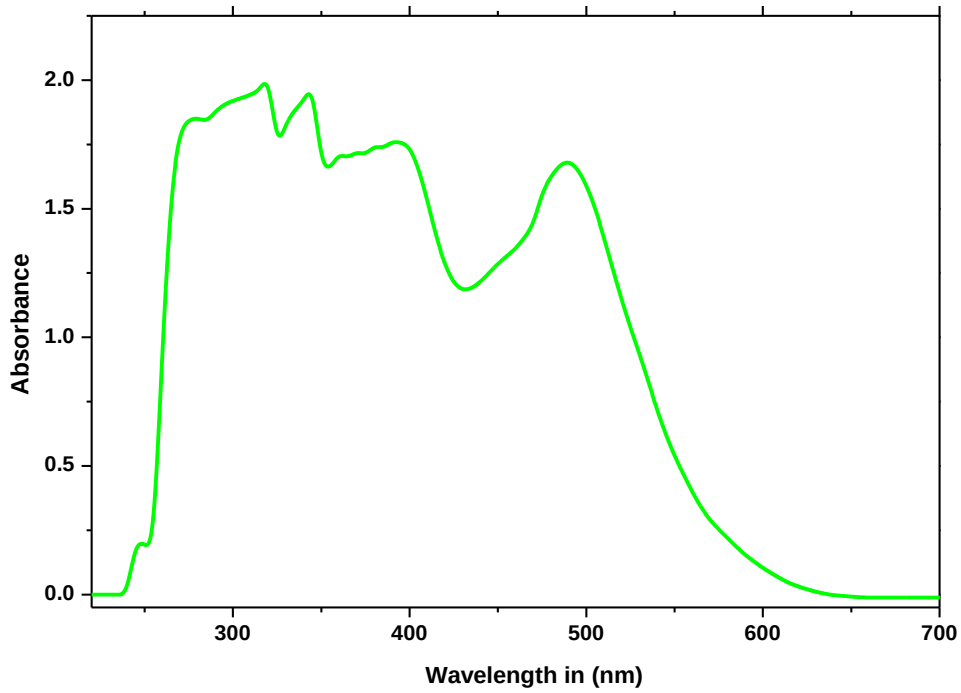

Figure S3. UV-visible spectra of compound MC2.

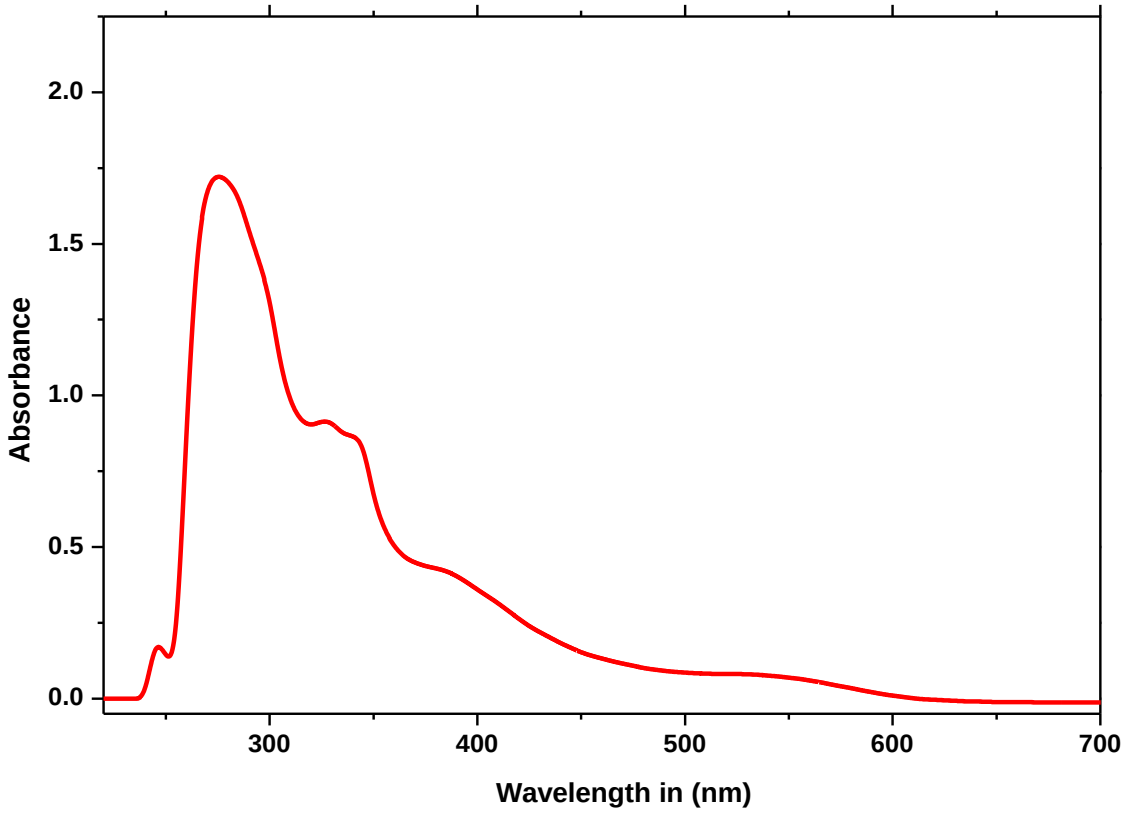

Figure S4. UV-visible spectra of compound MC3.

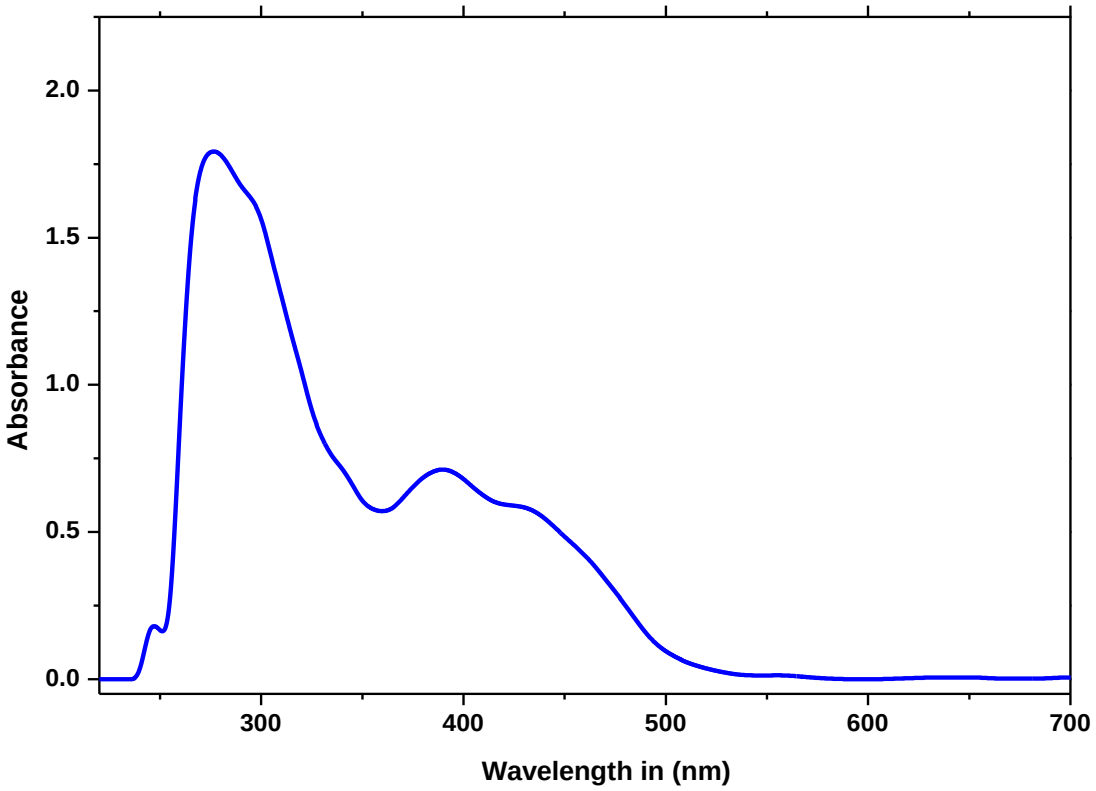

Figure S5. UV-visible spectra of compound **MC4.**

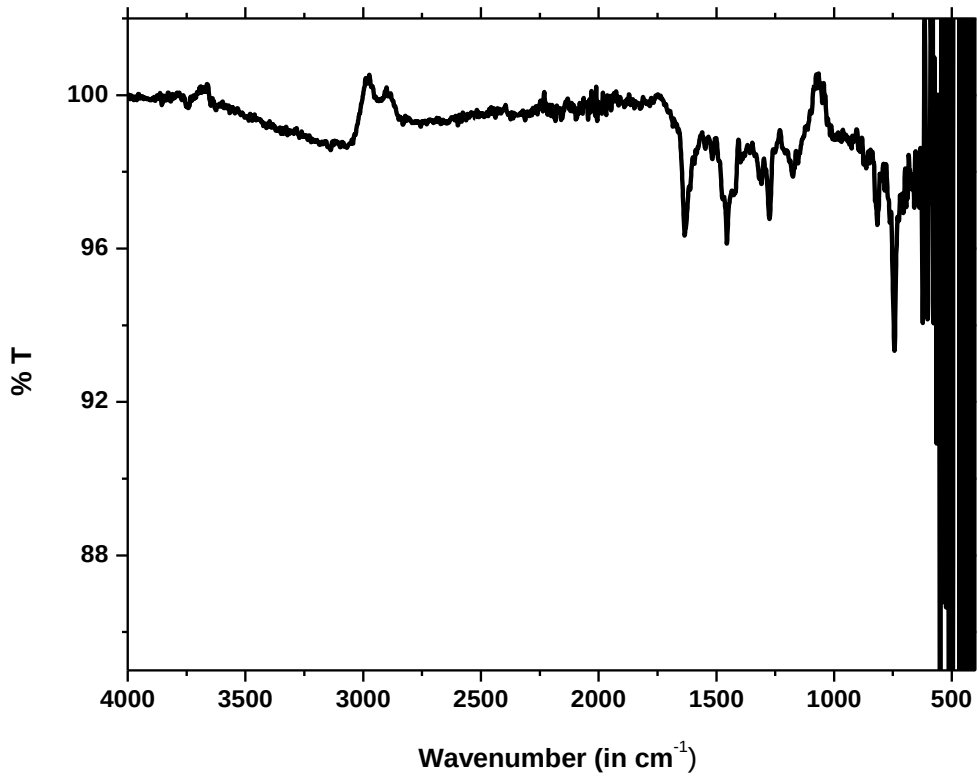

Figure S6. FTIR spectra of compound HBMB.

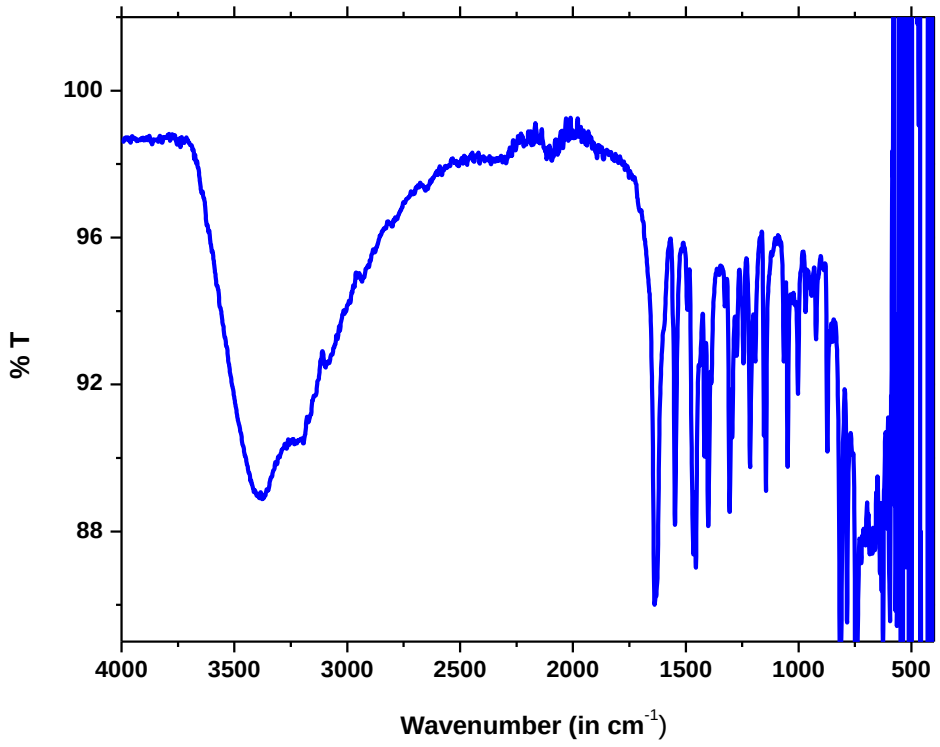

Figure S7. FTIR spectra of compound MC1.

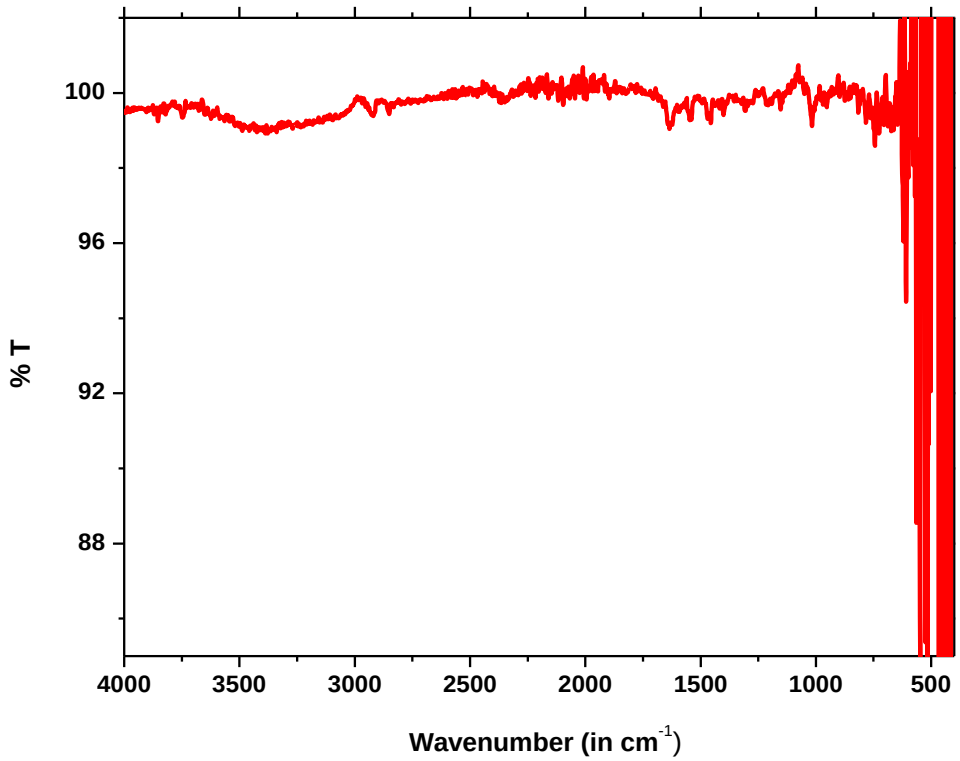

Figure S8. FTIR spectra of compound **MC2.**

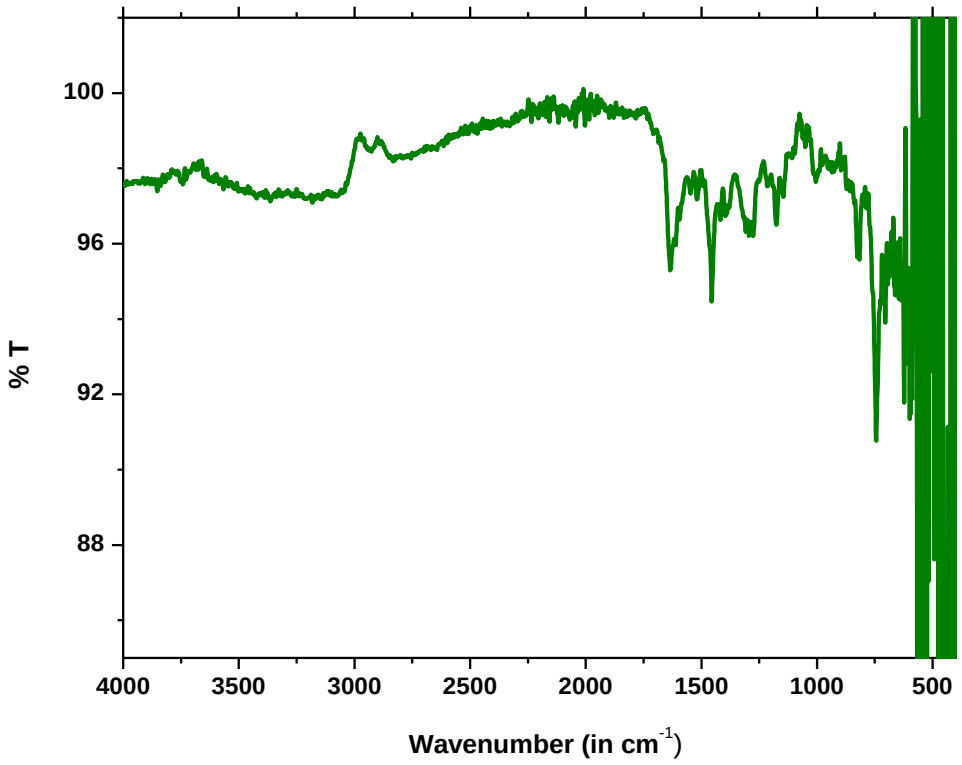

Figure S9. FTIR spectra of compound MC3.

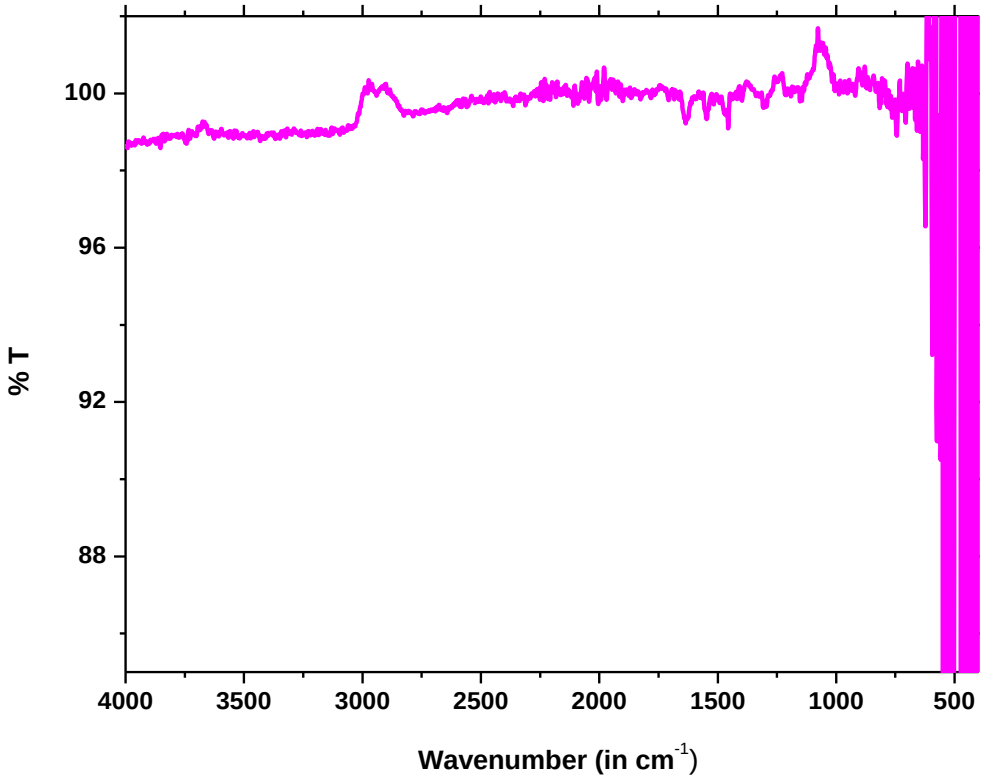

Figure S10. FTIR spectra of compound MC4.

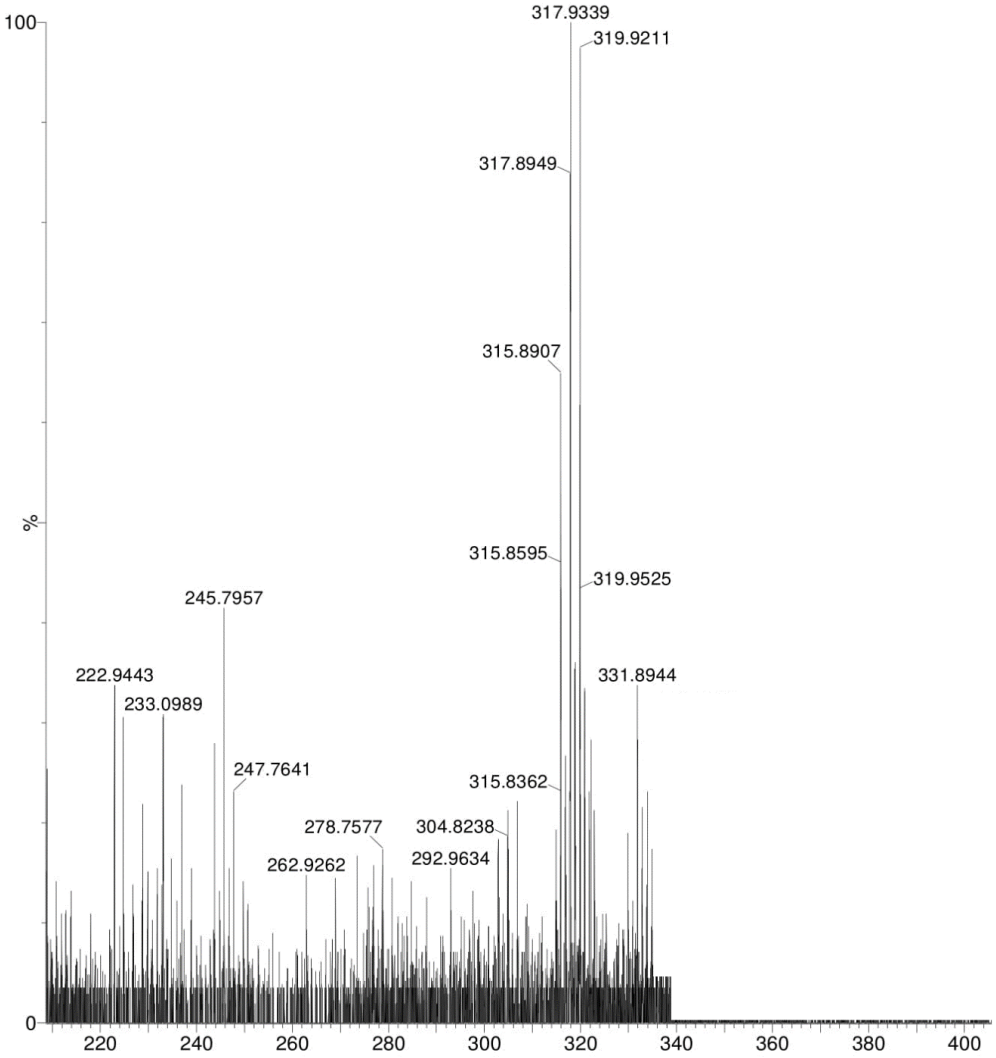

Figure 11. Mass spectra of compound **HBMB.**

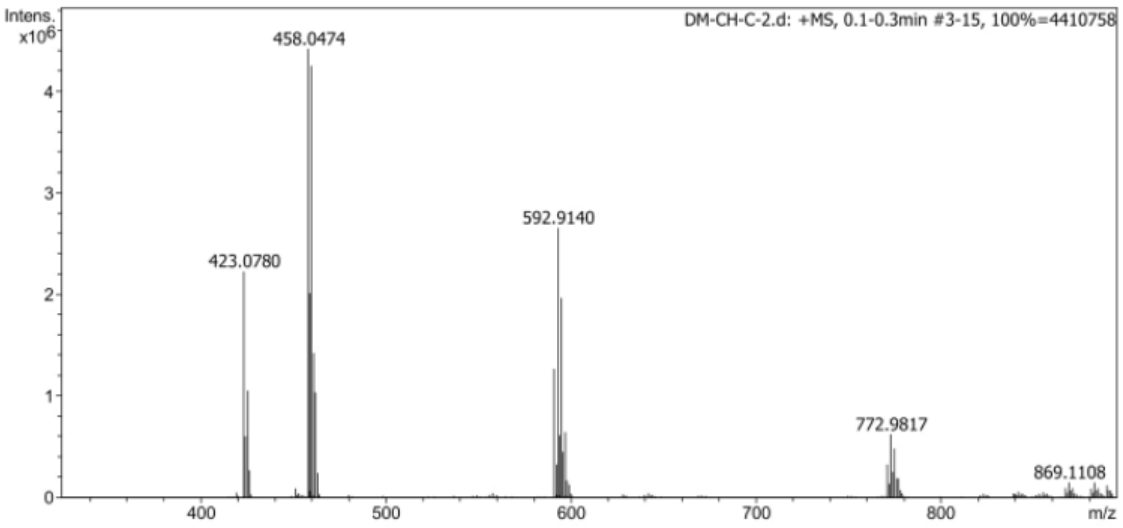

Figure S12. Mass spectra of compound MC1.

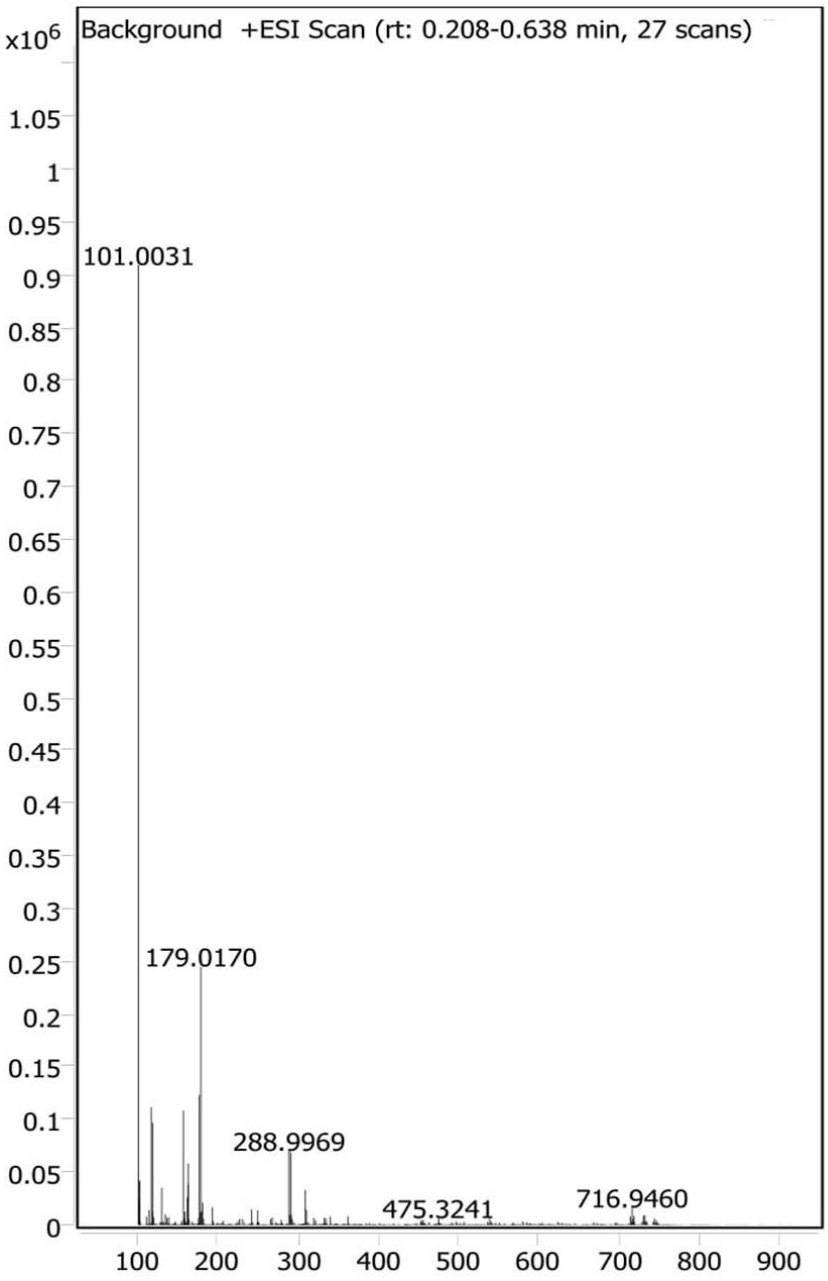

Figure S13. Mass spectra of compound MC2.

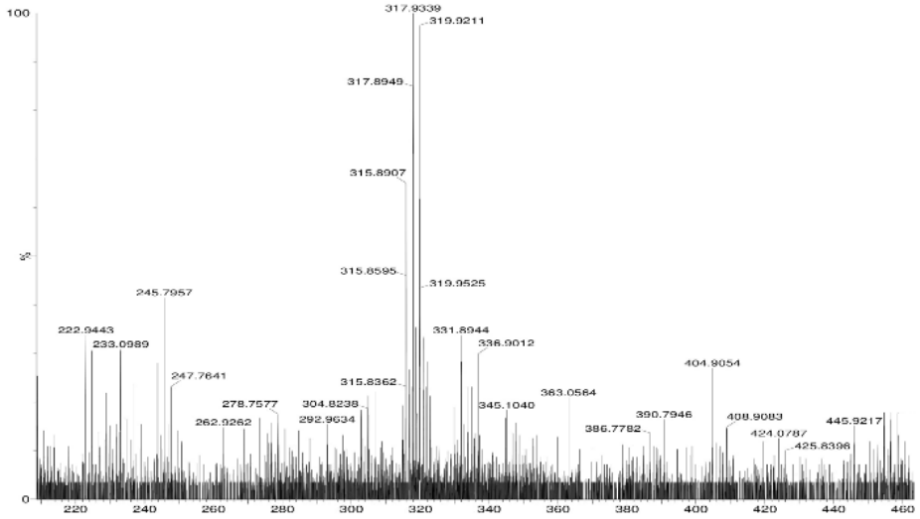

Figure S14. Mass spectra of compound MC3.

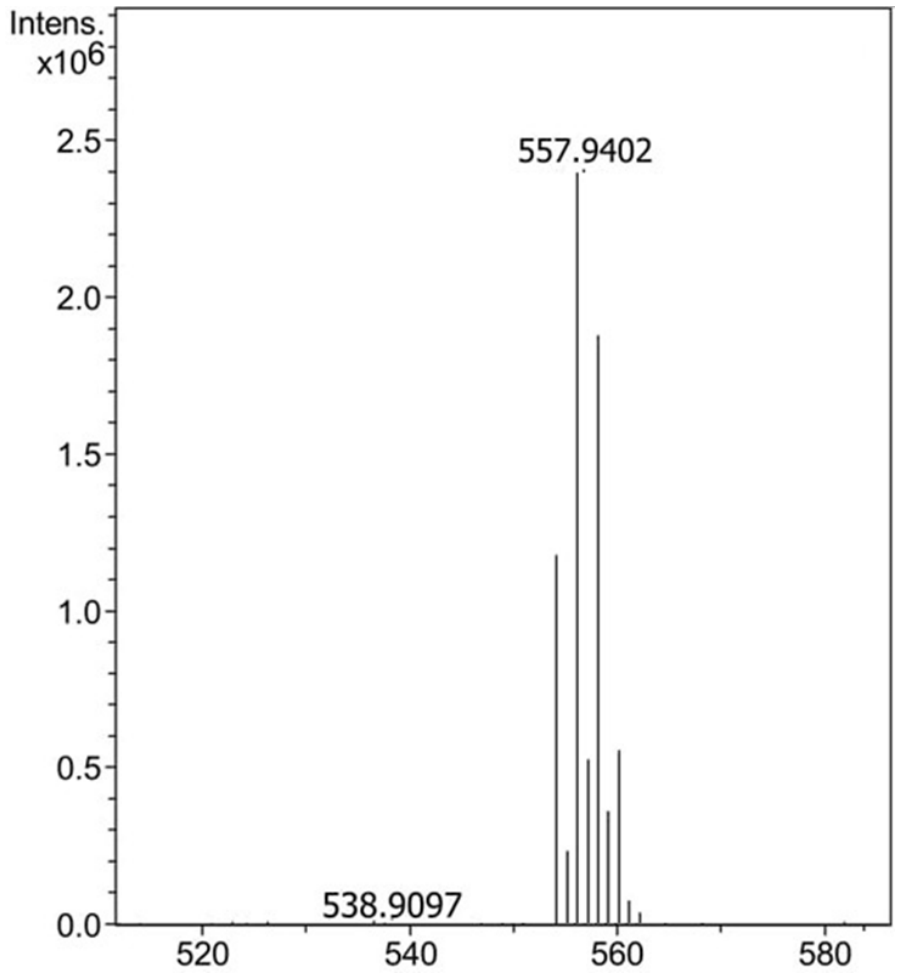

Figure S15. Mass spectra of compound **MC4.**

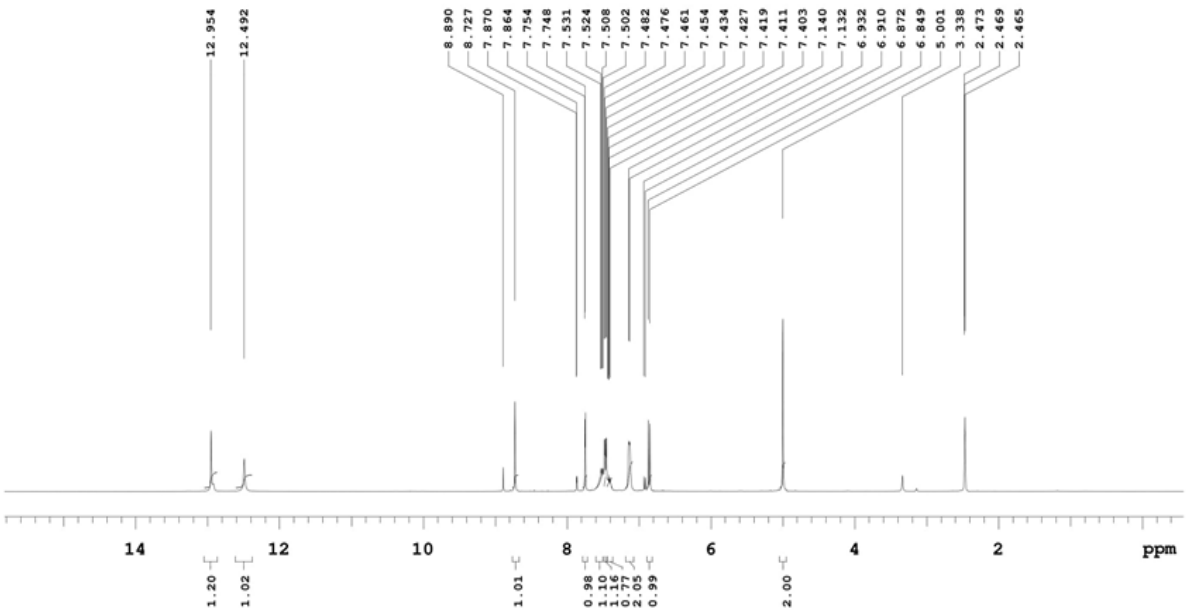

Figure S16. ^{1}H-NMR spectra of ligand HBMB.

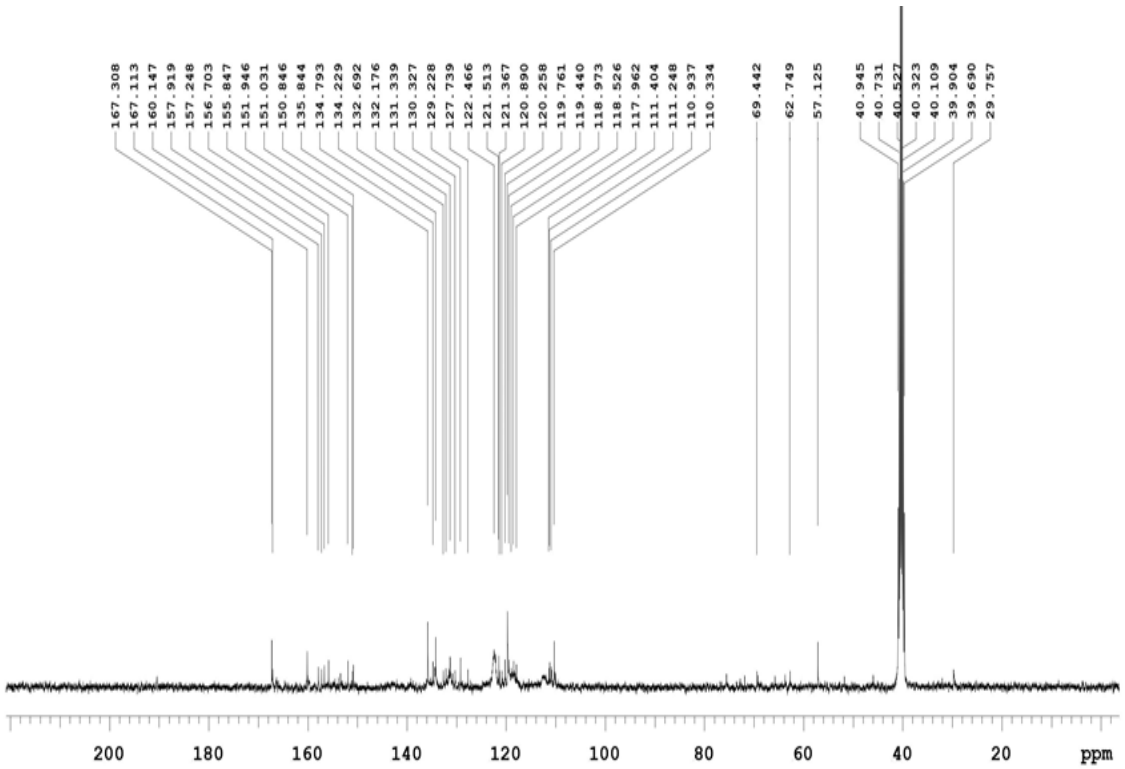

Figure S17. ^{13}CNMR spectra of ligand HBMB.

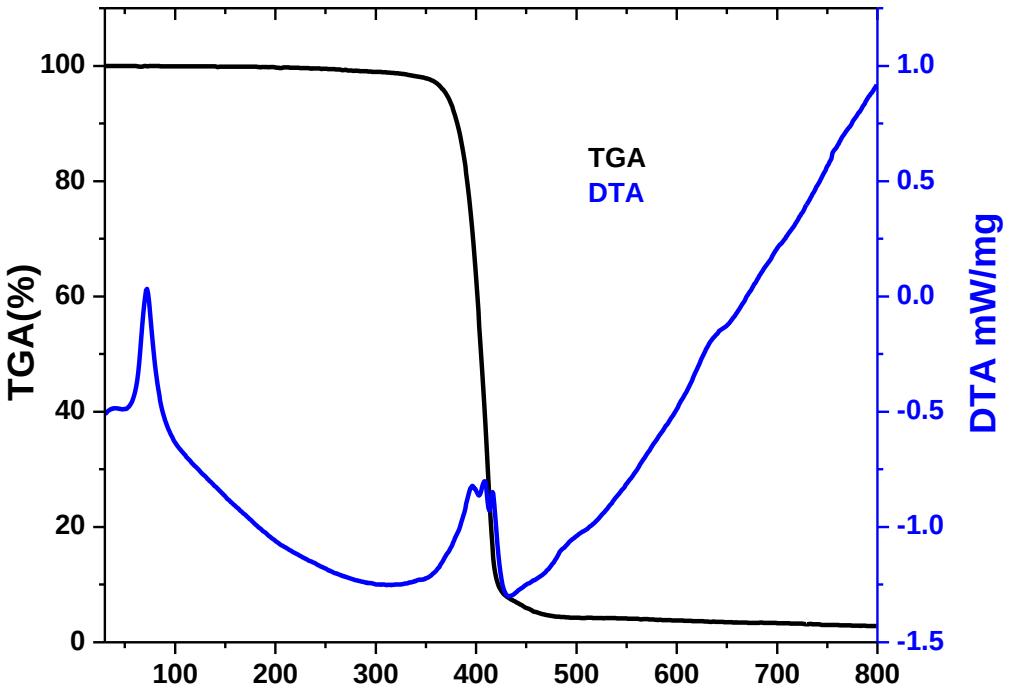

Figure S18. TGA and DTA for MC1.

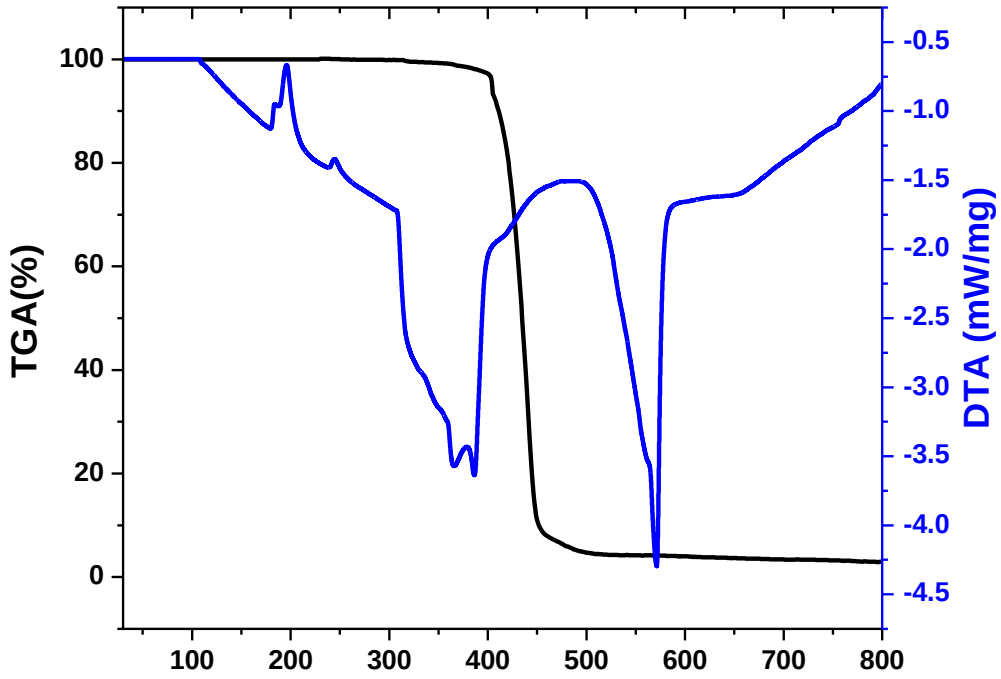

Figure S19. TGA and DTA for MC3.

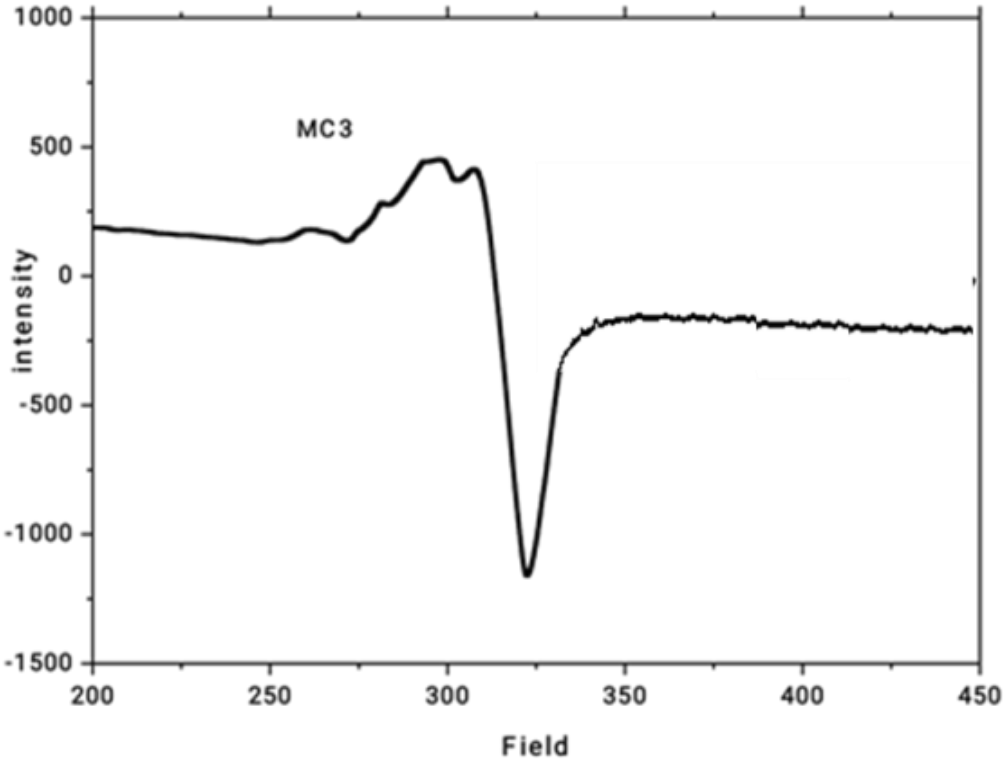

Figure S20. ESR spectrum of MC3 complex.

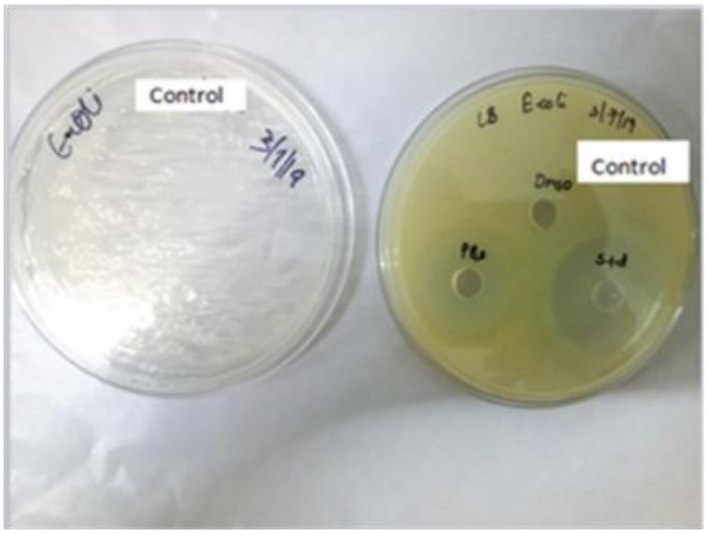

Figure S21. The bactericidal activity of control on *E. coli*.

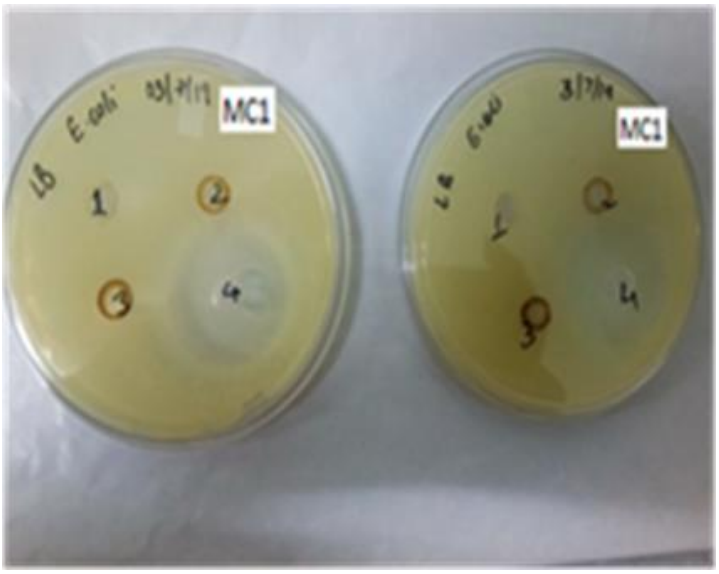

Figure S22. The bactericidal activity of MC1 on *E. coli*.

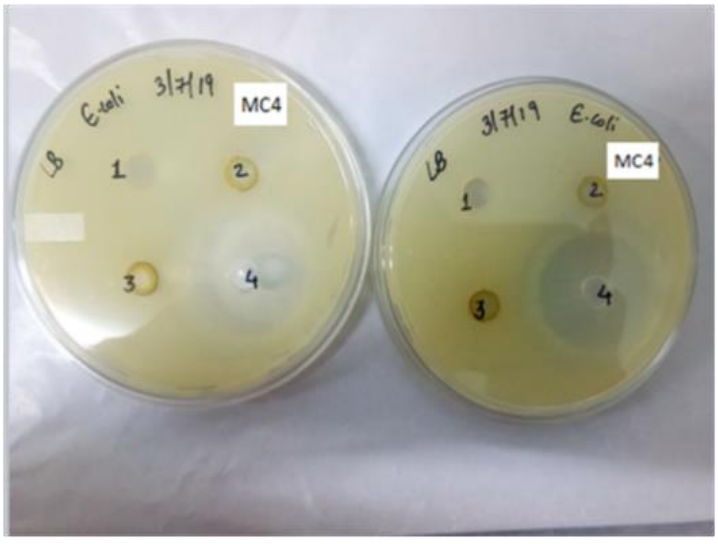

Figure S23. The bactericidal activity of MC4 on *E. coli*.

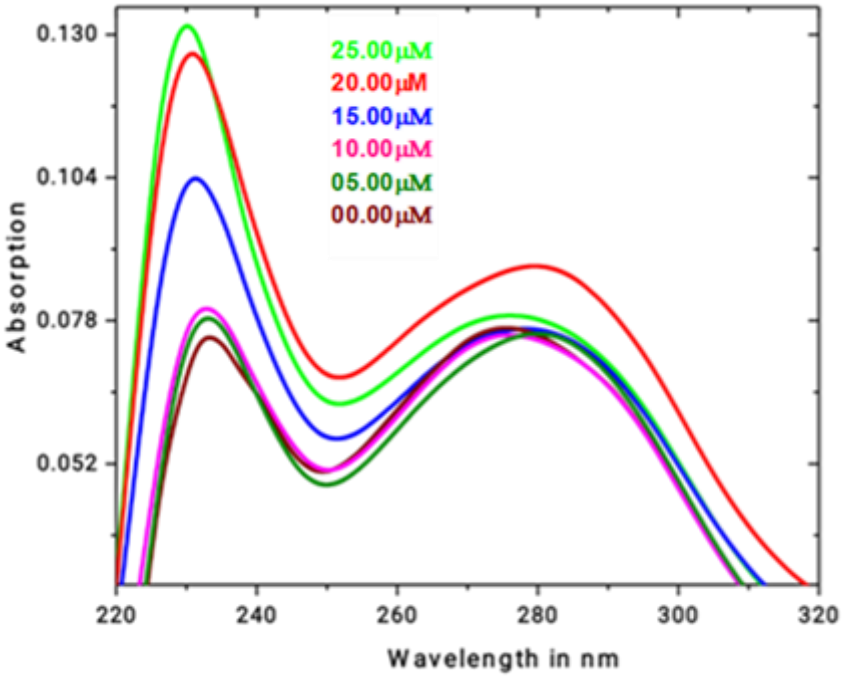

Figure S24. Absorption spectra of the complex (MC1) with different concentration of BSA; [MC1] = 25.00µM and [BSA] = 00.00-25.00µM at room temperature. The change in absorbance upon increasing concentration of BSA.

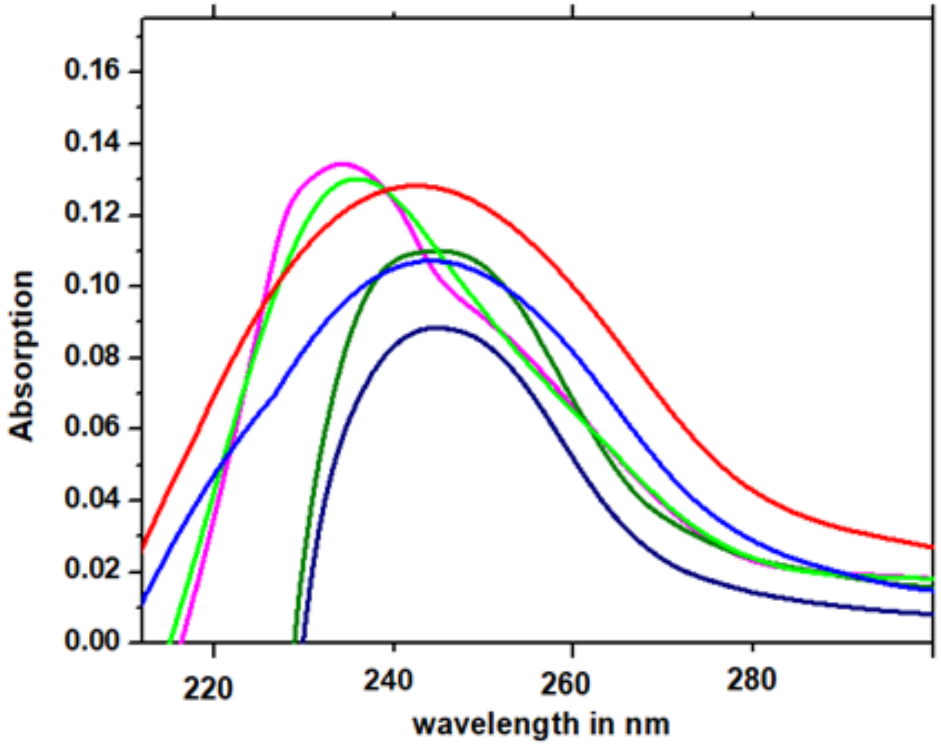

Figure S25. Absorption spectra of the complex (MC2) with different concentration of BSA; [MC2] = 25.00µM and [BSA] = 00.00-25.00µM at room temperature. The change in absorbance upon increasing concentration of BSA.

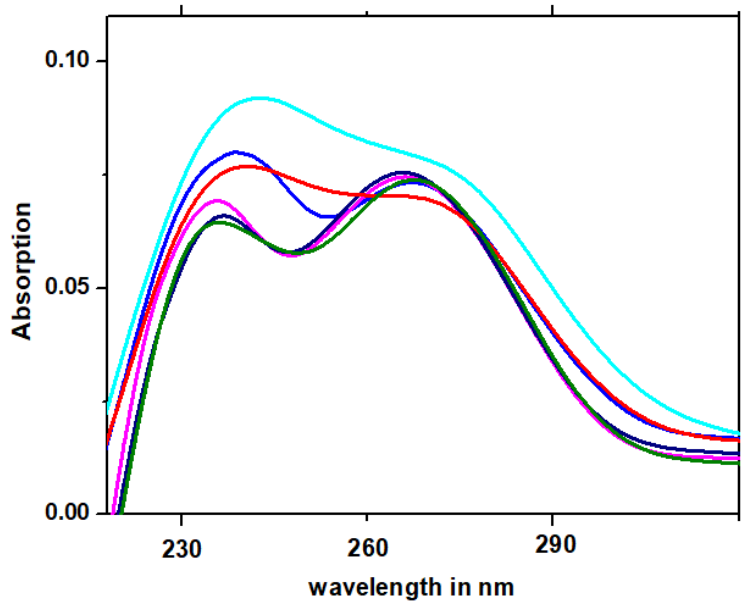

Figure S26. Absorption spectra of the complex (MC3) with different concentration of BSA; [MC3] = 25.00µM and [BSA] = 00.00-25.00µM at room temperature. The change in absorbance upon increasing concentration of BSA.

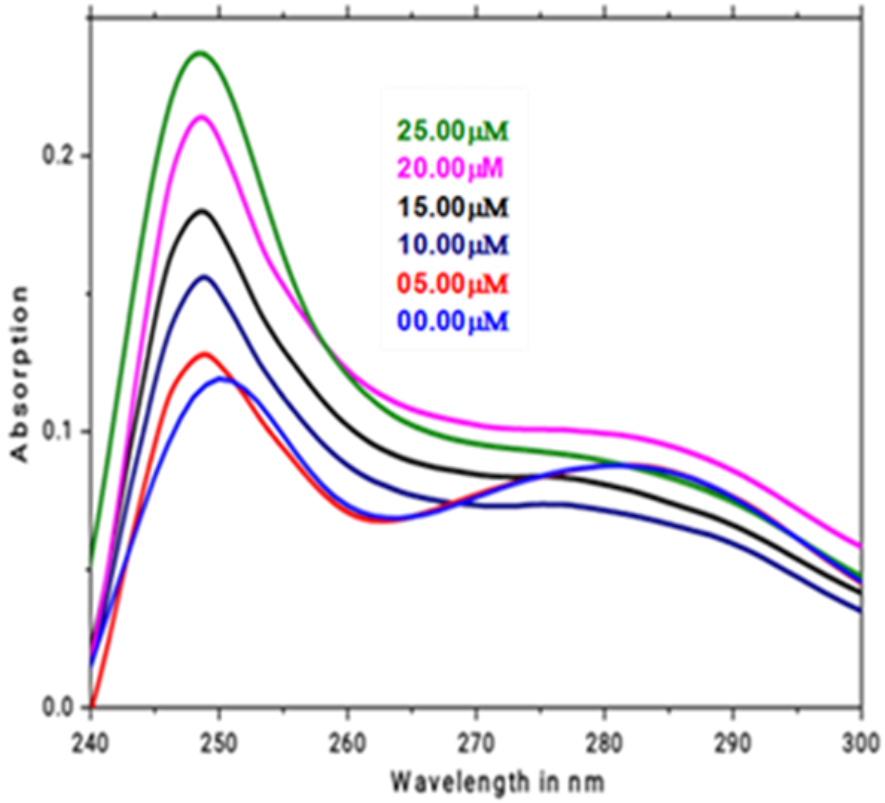

Figure S27. Absorption spectra of the complex (MC4) with different concentration of BSA; [MC4] = 25.00µM and [BSA] = 00.00-25.00µM at room temperature. The change in absorbance upon increasing concentration of BSA.

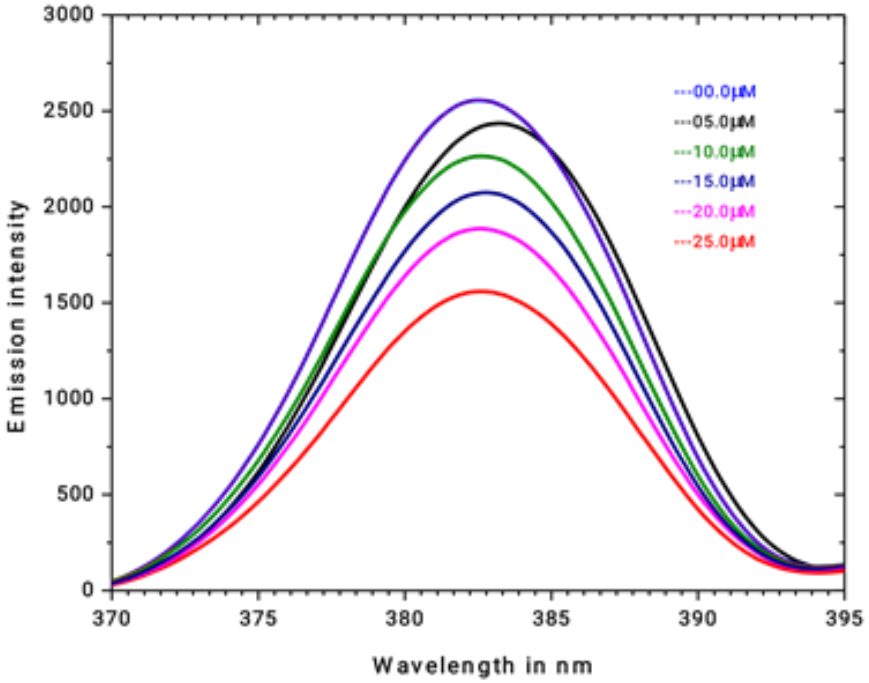

Figure S28. Fluorescence emission spectra of BSA in the presence of various concentration of complex (MC1); [BSA] = 10×10^{-6}M; [MC1] = 00.00-25.00μM at 05.00 μM increment.

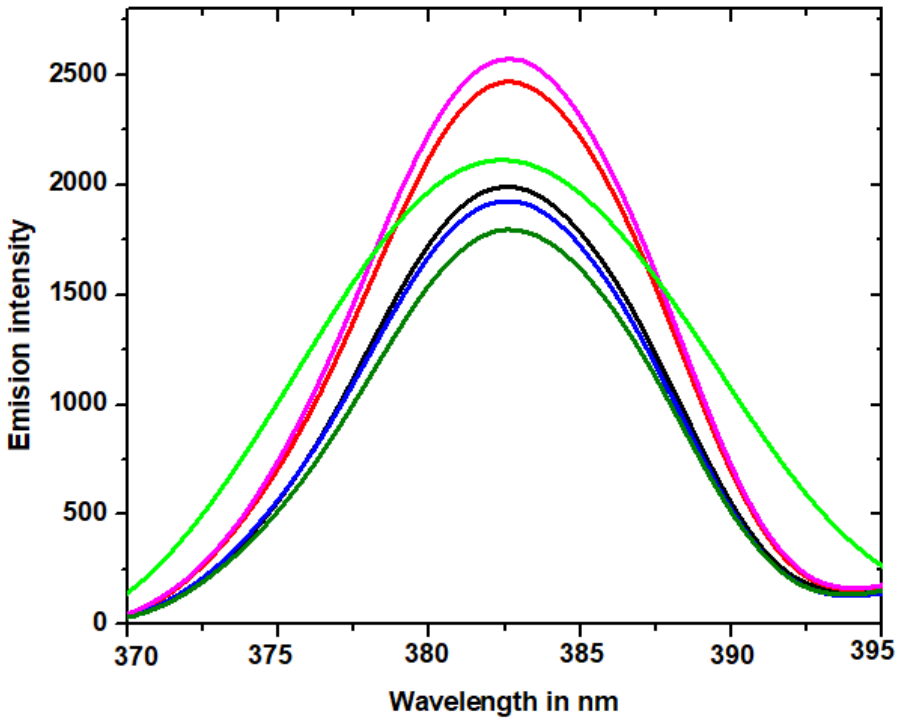

Figure S29. Fluorescence emission spectra of BSA in the presence of various concentration of complex (MC2); [BSA] = 10×10^{-6}M; [MC2] = 00.00-25.00μM at 05.00 μM increment.

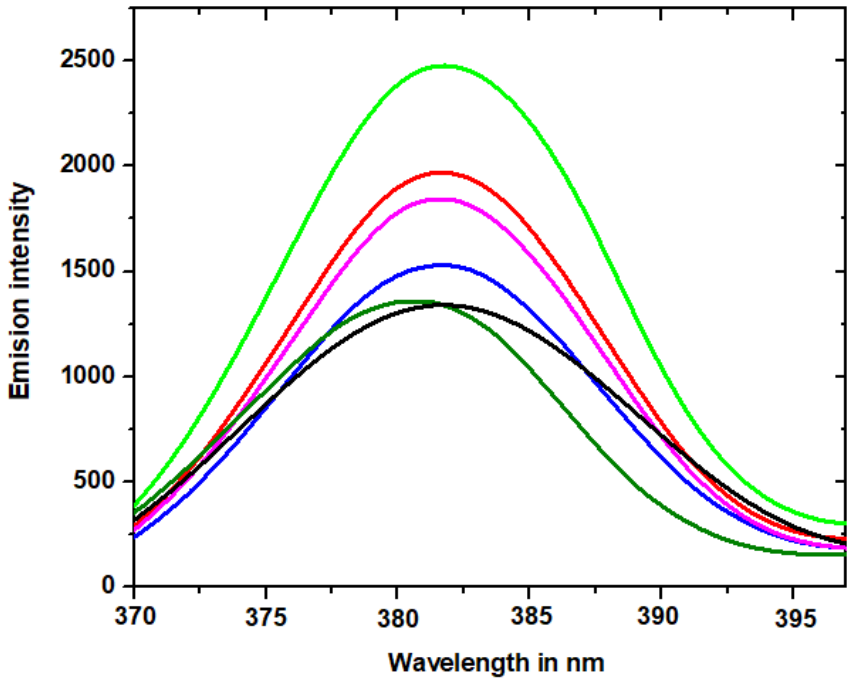

Figure S30. Fluorescence emission spectra of BSA in the presence of various concentration of complex (MC3); [BSA] = 10×10^{-6}M; [MC3] = 00.00-25.00µM at 05.00 µM increment.

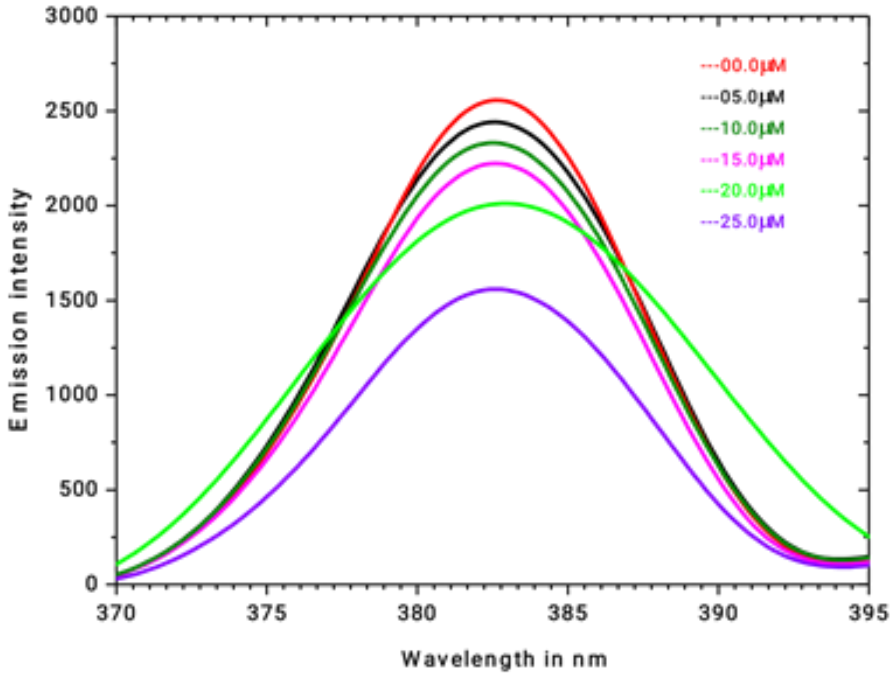

Figure S31. Fluorescence emission spectra of BSA in the presence of various concentration of complex (MC4); [BSA] = 10×10^{-6}M; [MC4] = 00.00-25.00µM at 05.00 µM increment.

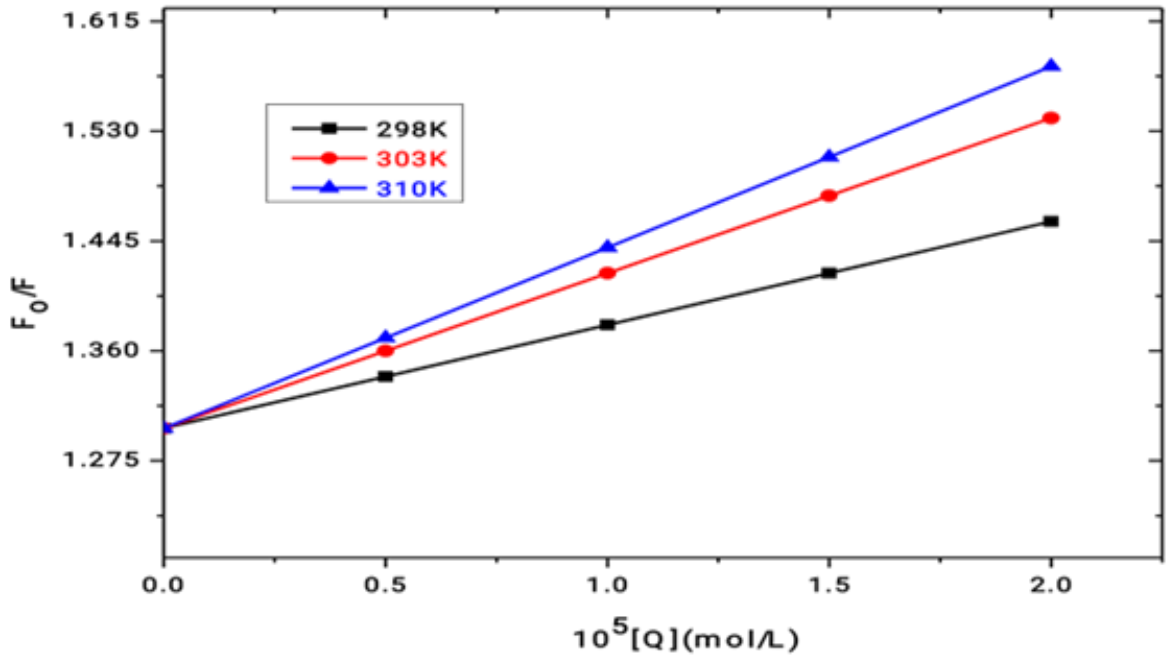

Figure S32. Ster-Volmer plot at different temperature.